Origin of EL3 chondrites: Evidence for variable C/O ratios during their course of formation—A state of the art scrutiny

A. EL GORESY[1,*], Y. LIN[2], M. MIYAHARA[3], A. GANNOUN[4], M. BOYET[4], E. OHTANI[5], P. GILLET[6], M. TRIELOFF[7], A. SIMIONOVICI[8], L. FENG[2], and L. LEMELLE[9]

[1]Bayerisches Geoinstitut, Universität Bayreuth, Bayreuth 95447, Germany
[2]Key Laboratory of Earth and Planetary Physics, Institute of Geology and Geophysics, Chinese Academy of Sciences, Beijing, China
[3]Department of Earth and Planetary Systems Science, Graduate School of Science, Hiroshima University, Higashi-Hiroshima 739-8526, Japan
[4]CNRS, UMR 6524,LMV, Clermont-Ferrand 63038, France
[5]Department of Earth Sciences, Graduate School of Science, Tohoku University, Sendai 980-8578, Japan
[6]École Polytechnique Féderale de Lausanne, Lausanne 1015, Switzerland
[7]Klaus-Tschira-Labor für Kosmochemie, Institut für Geowissenschaften, Universität Heidelberg, Heidelberg 69126, Germany
[8]ISTerre, UGA/CNRS, Observatoire des Sciences de l'Univers de Grenoble CS 40700, Grenoble Cedex 9 38058, France
[9]LGL-TPE, École Normale Supérieure de Lyon, UMR CNRS 5570 Lyon 69364, France
[*]Corresponding author. E-mail: ahmed.elgoresy@uni-bayreuth.de

Abstract–Mineral inventories of enstatite chondrites; (EH and EL) are strictly dictated by combined parameters mainly very low dual oxygen (fO_2) and sulfur (fS_2) fugacities. They are best preserved in the Almahata Sitta MS-17, MS-177 fragments, and the ALHA 77295 and MAC 88136 Antarctic meteorites. These conditions induce a stark change of the geochemical behavior of nominally lithophile elements to chalcophile or even siderophile and changes in the elemental partitioning thus leading to formation of unusual mineral assemblages with high abundance of exotic sulfide species and enrichment in the metallic alloys, for example, silicides and phosphides. Origin and mode of formation of these exotic chondrites, and their parental source regions could be best scrutinized by multitask research experiments of the most primitive members covering mineralogical, petrological, cosmochemical, and indispensably short-lived isotopic chronology. The magnitude of temperature and pressure prevailed during their formation in their source regions could eventually be reasonably estimated: pre- and postaccretionary could eventually be deduced. The dual low fugacities are regulated by the carbon to oxygen ratios estimated to be >0.83 and <1.03. These parameters not only induce unusual geochemical behavior of the elements inverting many nominally lithophile elements to chalcophile or even siderophile or anthracophile. Structure and mineral inventories in EL3 and EH3 chondrites are fundamentally different. Yet EH3 and EL3 members store crucial information relevant to eventual source regions and importantly possible variation in C/O ratio in the course of their evolution. EL3 and EH3 chondrites contain trichotomous lithologies (1) chondrules and their fragments, (2) polygonal enstatite-dominated objects, and (3) multiphase metal-rich nodules. Mineralogical and cosmochemical inventories of lithologies in the same EL3 indicate not only similarities (REE inventory and anomalies in oldhamite) but also distinct differences (sinoite-enstatite-graphite relationship). Oldhamite in chondrules and polygonal fragments in EL3 depict negative Eu anomaly attesting a common cosmochemical source. Metal-dominated nodules in both EL3 and EH3 are conglomerates of metal clasts and sulfide fragments in EH3 and concentrically zoned C-bearing metal micropebbles (≥25 μm ≤50 μm) in EL3 thus manifesting a frozen in unique primordial accretionary metal texture and composition. Sinoite-enstatite-diopside-graphite textures reveal a nucleation and growth

strongly suggestive of fluctuating C/O ratio during their nucleation and growth in the source regions. Mineral inventories, sulfide phase relations, sinoite-enstatite-graphite intergrowth, carbon and nitrogen isotopic compositions of graphite, spatial nitrogen abundance in graphite in metal nodules, and last but not least $^{129}I/^{129}Xe$ and $^{53}Mn/^{53}Cr$ systematics negate any previously suggested melting episode, pre-accretionary or dynamic, in parental asteroids.

INTRODUCTION

Enstatite chondrites (EC) comprise a distinct small group of undifferentiated meteorites characterized by formation at highly reducing conditions and dominance of stoichiometric troilite as the major sulfide mineral thus attesting their formation at very low fO_2 and also very low fS_2. The low dual fugacity is constrained by natural buffers, on one hand through the occurrence of native carbon and on the other hand by the assemblage stoichiometric troilite + kamacite in which the activity of FeS in troilite is close to unity. The common highly reduced stage was thought to be indicative of a single common source asteroid (Keil 1968; Kong et al. 1997). In contrast, there is convincing evidence that individual members indeed emerged from different parental asteroids (Sears 1980; Ehlers and El Goresy 1988; El Goresy et al. 1988; El Goresy and Ehlers 1989; Lin and El Goresy 2002). The dual buffered fugacity dependence was unfortunately not recognized in numerous publications over the last decades (Rubin et al. 1997; Humayun et al. 2009; Rubin and Wasson 2011; Horstmann et al. [2014], and references therein).

The total number of enstatite chondrites does not exceed 2% of the number of diverse chondritic meteorites. Place of birth and mechanisms of formation of their unequilibrated members (EH3 and EL3) have been debated since 1983. It is disputed if the unequilibrated E-chondrite members are solar condensates (Lin and El Goresy 2002; El Goresy et al. 2011b; Weisberg and Kimura 2012), resulted from impact melting of already accreted parental proto-asteroids (Horstmann and Bischoff 2014), or emerged from unknown pre-accretionary melts (Horstmann et al. 2014). This long-lasting disagreement emerges from several sources:

1. Lack of comprehensive recognition of the *menagerie* of the exotic and unusual sulfide assemblages, lack of knowledge of crucial details of mutual growth textures, and their cosmochemical relevance;
2. Sharp contrast in the petrographic background of investigators and relevance of their interpretation;
3. Sharp contrasts in evaluating the relevance of the co-existing diverse compatible sulfide assemblages and their experimentally established phase relations;
4. The unusual sulfide inventory of enstatite chondrites is far from known to many meteoriticists specialized in silicate systems. Furthermore, djerfisherite, an important EH-sulfide and a radiometric carrier for ^{40}K-^{40}Ar, ^{87}Rb-^{87}Sr, and ^{36}Cl-^{36}S systems is unrecognizable from troilite at BSE-SEM (e.g., McKinley et al. 1984). General lack of knowledge of mineralogical details of expected sulfide assemblages at high C/O ratio impedes a scholarly characterization of the meteorite under investigation;
5. Scarcity or lack of nanoscale isotopic investigations.

These shortcomings and lack of overall meaningful understanding of the encountered mineralogy accompanied the ongoing research for several decades. The diverse triggers of disagreement call for comprehensive revision of the mineralogical and cosmochemical investigations thus aiming a clarification of ambiguities and erasing discrepancies. We hence considerably revised our methodology to include nano-scale isotopic investigation techniques and careful checking if the proposed interpretations are not discrepant with petrologic findings and results of short-lived isotopic systems. Our revised methodology is indeed capable of addressing many of the controversies; discarding unreliable genetic interpretations; and thus diminishing, removing, and narrowing down the numerous disagreements.

The low fO_2 induced a considerable shift of the geochemical behavior of nominally lithophile elements like Mg, Ca, Ti, Mn, Cr, K, Na, and the REE thus leading to their occurrence either as individual sulfides (Ca and majority of the REE in oldhamite, Mn in alabandite in EL chondrites or in either niningerite or keilite in EH chondrites, Cr in daubréelite, K in djerfisherite, Na and Cr in caswellsilverite, and the major portion of Mg in niningerite or keilite in EH; Ramdohr 1963, 1973; Keil 1968; Larimer and Bartholomay 1979; El Goresy et al. 1988; Lodders and Fegley 1993; Lin and El Goresy 2002; Gannoun et al. 2011). The exotic cosmochemical behavior and mineral assemblages are distinct from what is present in ordinary chondrites (OC) and carbonaceous chondrites (CC).

However, texturally, primitive enstatite chondrites, like in unequilibrated OC and CC, contain two or three

distinct mineral lithologies (1) chondritic lithology; (2) polygonal silicate-rich objects dominated by wickerwork of idiomorphic enstatite crystals with minor diopside; and (3) metal-dominated but silicate-, graphite, and sulfide-bearing nodules and/or metal fragments.

The stark reducing conditions were predicted to have resulted from high C/O ratio in their source regions from which they are inferred to have emerged in the solar nebula first by Larimer and Bartholomay (1979) and later addressed in detail by Lodders and Fegley (1993). This interpretation was supported by recognition of a specific mineral inventory that is compatible with low fO_2 and characteristic of many EC members: namely oxidized iron is a minor to diminishing constituent in olivine and pyroxene, the latter occurs as almost pure enstatite along with minor diopside both containing minor concentrations of MnO (Ramdohr 1963, 1973; Keil 1968; Kallemeyn and Wasson 1986; El Goresy et al. 1988, 2015; Lin and El Goresy 2002; Weisberg and Kimura 2012). Furthermore, a distinct inventory registers abundant titanian-chromian troilite (FeCrTi)S, subordinate oldhamite (CaS), niningerite (MgFeMn)S or keilite (FeMgMn)S, alabandite (MnFeMg)S, minor manganoan sphalerite (ZnFeMn)S, djerfisherite $(KNa)_6(FeCuNi)_{25}S_{26}Cl$), caswellsilverite $NaCrS_2$, zincian daubréelite $(FeZnMn)Cr_2S_4$, pentlandite $(FeNi)_9S_8$, chalcopyrite $CuFeS_2$, cubanite Cu_2FeS_3, schreibersite $(FeNiCo)_3P$, perryite $(NiFe)_5(SiP)_2$, and lawrencite $FeCl_2$. Various graphite morphologies encountered in the different lithologies of the same EH or EL enstatite chondrites bears witness of various formational origins at the high C/O ratios (see details in the Petrography section). This mineral inventory not only on the one hand diagnostically sifts out EC from ordinary and carbonaceous chondrites, but also on the other leads to recognition of the two distinct subgroups EH and EL in which for example, niningerite and keilite are, with few exceptions, confined to EH members, whereas alabandite is present mainly in EL.

It is generally accepted that ECs comprise two subgroups: EH high Fe, high siderophile subgroup and EL low Fe, low siderophile subgroup (Sears 1980; El Goresy et al. 1988; Lin and El Goresy 2002; Gannoun et al. 2011; Weisberg and Kimura 2012). The two subgroups have not only some important common lithologies resulting from the common high C/O ratios but also clear diagnostic differences emerging from their comparatively distinct elemental inventories. EH and EL are also characterized by the differences in the Ni- and Si- contents of kamacite and taenite (Keil 1968; El Goresy et al. 1988; Lin and El Goresy 2002). EL contains a unique minor component but genetically of great cosmochemical and potentially isotopic relevance, namely the silicon oxinitride sinoite Si_2N_2O first discovered by Andersen et al. (1964) in some equilibrated members of the EL subgroup. It stores important information on the involvement of N_2 during the course of their nucleation and growth in the source regions and also hints at its possible formational mechanism in primitive and equilibrated EL members. The metal alloys kamacite and taenite also sequester moderate amounts of Si and P whose concentrations are characteristic for EH and EL, respectively (e.g., Lin and El Goresy 2002).

Thermodynamic calculations by Larimer and Bartholomay (1979) and Lodders and Fegley (1993) predict oldhamite (CaS) as an early condensate from the solar gas at ($P^{tot} = 10^{-3}$ atmosphere) and at a high C/O ratio. A recent compilation of thermodynamic calculations at ($P^{tot} = 10^{-4}$ atmosphere) by Grossman et al. (2008) reveals in contrast condensation temperatures and sequences of the mineral constituents are different from those obtained by Lodders and Fegley (1993). Grossman et al. (2008) emphasize that mineral stabilities and associations predicted from their calculations also deviate from what is encountered in EH3 chondrites. They emphasize that "some thermodynamic data for the exotic phases present in E-chondrites are uncertain by sufficient amounts that stability fields for oldhamite (CaS) and MgS may exist at a C/O ratio where enstatite formation occurs at a higher temperature." We stress the notion that Grossman et al. (2008) tested the consistency of their predictions with natural inventories for the EH3 chondrites only. Neither the calculated condensation sequence by Lodders and Fegley (1993) nor that by Grossman et al. (2008) deliver any straightforward quantitative detail that matches what we encounter in natural assemblages in unequilibrated EH3 and EL3 chondrites (El Goresy et al. 1988, 2015; Gannoun et al. 2011; Lin and El Goresy 2002; Weisberg and Ebel 2015). Many of the species predicted in both calculations are present in EH3 and/or EL3 chondrites, albeit in different intergrowths and sequence not forecasted by both predictions. Oldhamite-enstatite-diopside assemblages occur both in EH and EL in chondrules and lithological units in matrices and hence cannot have been produced by the same mechanism in these different lithologies. Textures of natural oldhamite-, diopside-, and plagioclase-bearing assemblages even contradict both predicted schemes. Lodders and Fegley (1993) predicted that CaS commences to condense in the solar nebula at 1379 K from a gas of solar composition and that it should react with the cooling solar gas below 1280 K to form diopside and/or anorthite. In contrast, calculations by Grossman et al. (2008) foresee that Ca-rich pyroxene

condensate should react with $H_2S_{(g)}$ to form oldhamite. Such reactions call for occurrence of textural evidence for one or the other proposed reactions. The first scenario implies occurrence of diopside and/or anorthite replacing oldhamite, whereas the second in contrast calls for diopside replacement by oldhamite. We have never encountered textural or cosmochemical evidence for the two predictions. In addition, should oldhamite have emerged from the reaction of diopside with the solar gas or alternatively, diopside from reaction of oldhamite with the solar gas, the REE budget and patterns of both oldhamite and diopside should be similar. Such an REE similarity between oldhamite and diopside was not encountered in any EH or EL so far. Furthermore, Grossman et al. (2008) predicted enstatite formation by reaction of both previously condensed forsterite and sinoite with the solar gas thus entirely exhausting sinoite and producing enstatite. However, we have never encountered in EH3 or EL3 any texture reminiscent of a reaction involving all the three species forsterite, sinoite, and enstatite. Interestingly, in comparison, we indeed encounter sinoite only in metal nodules in EL3 chondrites enclosed and progressively consumed by enstatite and/or diopside but the reaction textures do not match in detail the predictions by Fedkin and Grossman (2006) and Grossman et al. (2008). In short, there are significant discrepancies between thermodynamically predicted gas-solid reactions, condensation sequences, and natural mineral assemblages encountered in both unequilibrated EH3 and EL3 chondrites. Accordingly, we emphasize that achieving a meaningful scheme explaining the formational conditions and growth sequence of constituents of unequilibrated ECs can only rely on detailed comprehensive documentation of the mineral inventories and meaningfully evaluating them, their stabilities, and specifically detailed intergrowth textures in the pertinent meteorites.

According to Lodders and Fegley (1993), the *earliest* CaS condensates from a gas of strictly solar composition and high C/O ratio should incorporate REE as sulfides according to their volatilities with CI-normalized REE patterns depicting negative anomalies in the less refractory Eu and Yb. They also predict that between 1379 K and 1280 K all REE sulfides, except GdS, must be incorporated in oldhamite. GdS should individually condense at 1418 K. The temperature interval between 1379 K and 1280 K should then record the abundance of the REE incorporated in the individual oldhamite crystals and the fine-scale condensation and accretion episodes in the different oldhamite assemblages thus eventually reflecting the REE inventory of the inferred solar gas at the brink of oldhamite condensation (see e.g., assemblages listed in Table 4 in El Goresy et al. 1988). REE fractionation is less in a gas with a high C/O ratio and solar abundance because most of the REE and the actinides are expected to directly condense as sulfides into oldhamite within few degrees of CaS condensation (Lodders and Fegley 1993). Consequently, the REE abundance in oldhamite earliest condensates should display very similar patterns with Eu and Yb depletions in both unequilibrated EH3 and EL3 provided that earliest oldhamite condensates emerged from the region with REE solar abundance. With few exceptions, any fractionation between the REE in oldhamite could only be produced according to Lodders and Fegley (1993) "by removing it after its condensation from equilibrium with the nebular gas." The published REE patterns in oldhamite in unequilibrated EH3/4 chondrites (finds and falls) fall according to Lundberg et al. (1989), Crozaz and Lundberg (1995), and Gannoun et al. (2011) into three diverse categories (1) unfractionated flat patterns, (2) relatively unfractionated flat patterns with Yb excesses, and (3) relatively unfractionated flat patterns with both Yb and Eu excesses. We tag the latter pattern type as the *mainstream* REE pattern for EH3 chondrites because it is the dominant pattern in oldhamite in this subgroup. Gannoun et al. (2011) and Lodders and Fegley (1993) tentatively interpret Yb or Yb + Eu excesses in oldhamite as a result of additional condensation of Yb or Yb and Eu from another nebular reservoir into an oldhamite with originally flat pattern. This could, according to Lodders and Fegley (1993) result either from gas or grain transport. Both the thermodynamic calculations and the REE abundance measurements in petrologically sketchy-described oldhamites in EH chondrites. Crozaz and Lundberg (1995) demonstrate not only the cosmochemical potential of oldhamite but also in detail the inconsistencies between calculations and natural occurrences. This calls for comprehensive scrutiny and an accurate petrologic characterization of mineral inventories, intergrowth textures and REE abundances not merely listing the minerals encountered without textural details. REE patterns in oldhamite in EH3 and EL3 are apt to develop to a powerful cosmochemical tool allowing us to unambiguously recognize EH3 and EL3 source regions, and importantly to inspect if the source regions from which oldhamite in EH3 and EL3 originated are media with strictly REE solar abundance; REE differently fractionated solar gas reservoirs; or alternatively resulted from partitioning between oldhamite, other sulfides, and silicates during dynamically controlled melting events, melting in a pre-accretionary episode, or merely of secondary origin induced during weathering and long residence in finds in Antarctica or North West Africa thus resulting in

selective removal of certain REE. It is worthwhile to mention that the latter possibility was not considered to be of importance.

In addition, textural details of feathery graphite fans, offer a unique possibility to scrutinize at high magnification their morphology, the fine-scale nature of the adherence of individual graphite crystallites in the fans, and to inspect if these crystallites nucleated adhering to each other or grew on pre-existing mineral species thus allowing shedding light not only on the nucleation sequence but also on the C/O ratio in the medium at the brink of nucleation of the graphite fans. Graphite nucleation on pre-existing species can suggest a mark pointing to increase in the C/O ratio in the medium at the given total pressure and temperature. See details in the section on petrography of metal nodules.

In contrast to the condensation models discussed above, Rubin and Wasson (2011), Keil (2007), Van Niekerk and Keil (2011) and several references therein suggest that both graphite books and sinoite grains in EL4-6 chondrites originated by impact melting of unknown precursors followed by selective CaS melt migration "for few centimeters." This scenario was also adopted by Humayun et al. (2009) and Bischoff et al. (2010) and later considerably modified by Horstmann et al. (2014) to another melting mechanism but involving unconstrained "pre-accretionary" events and discarding the impact melting mechanism previously adopted by them as well. The impact melting scenario was recently convincingly demonstrated to be fully discrepant with petrography of both EH and EL chondrites (Lin and El Goresy 2002; Gannoun et al. 2011). Such a dynamically induced melting mechanism would also have totally erased all mineral textures inverting them to igneous-like settings; destroyed chondrules; erased the cosmochemical complementarity; induced chemical homogenization; and revealed high-pressure phase transformations of olivine, enstatite, diopside, and graphite in the first place. This, as we also will show below, is never observed in any unequilibrated EH3 or EL3 or any equilibrated enstatite chondrite either, the latter declared by such scenario to be "impact-melt rocks" (Bischoff et al. 2010).

Research procedures may lead to a meaningful result if they, in the first place, relied on meticulous and skillful petrographic investigations, and specifically addressed the following important issues:

1. Were REE abundances at the brink of oldhamite nucleation strictly solar or fractionated in the regions or media where CaS commenced to nucleate, grow, and accrete into EH and EL chondrites?
2. If fractionated, is it different in EH and EL chondrites and how?
3. Do the growth textures of the encountered primordial assemblage oldhamite, sinoite, enstatite, and graphite in EL3 chondrites agree with the sequences and gas-solid reactions predicted by the condensation calculations of Lodders and Fegley (1993) and/or Grossman et al. (2008)?
4. Do the encountered growth textures of these primitive E chondrites reveal information conducive of change in the C/O ratio during the course of nucleation in the source regions from which they emerged? To more reducing conditions? Vice versa? And if so at what stage?
5. What are the C- and N-isotopic signatures of various graphite morphologies and if possible the N-isotopic compositions of coexisting sinoite in the same EL3 chondrite?

Proposal for a Stark Revised Research Strategy

The major aim is uncovering comprehensive details of the nucleation, intergrowth sequence, and accurate inventory of the present minerals and specifically documenting mineral replacement or consumption textures. These should reveal genetic information of the origin and formational mechanisms of EL3 chondrites. Proposed formational mechanisms of ECs were hampered over several decades by contrasting and controversially debated reports, unconstrained and in part speculative suggestions leading to stark discrepant interpretations. With few exceptions, many of the published articles concentrated on general issues merely leaning on comparison with OC and CC chondrites, and ignoring crucial ones, specifically the relevance of low fO_2, fS_2, missing published important reports, and unaware of the importance of C- and N-isotopic compositions of all graphite morphologies in the same meteorite. Recent SIMS investigations revealed, for example, robust evidence for C-, N-, and H-isotopic signatures of graphite (Mostefaoui et al. 2005) in chondritic meteorites unfortunately unknown to few EC scholars thus calling for application of this important procedure specifically to graphite morphologies in ECs. Of special relevance is a realistic characterization of the nature and composition of metal nodules and metal fragments in using high contrast at BSE-SEM to disclose in detail its components, texture, and compositions. For this reason and to overcome other shortcomings outlined above, we profoundly revised our research procedure thus developing a considerably detailed scheme that enables addressing petrologic, fabric, and specifically isotopic diagnostic issues. The unique mineral inventory, the extremely reducing conditions prevailed during the formation of individual EC types and their variability even on microscopic

scales in comparison to OC and CC call for improved research strategies.

The mineral inventories outlined above are apt to uncover more key information on diverse textures of the same mineral in different assemblages, fO_2, fS_2, and REE patterns in oldhamite if fingerprinting the source regions and their REE signatures, recognizing parental asteroids in which they accreted and eventually equilibrated, if in a single asteroid as advocated by or in recognizable different individual asteroids (Ehlers and El Goresy 1988; El Goresy et al. 1988; Gannoun et al. 2011) and their thermal histories (Skinner and Luce 1971; Ehlers and El Goresy 1988; and references therein). We emphasize the fact that, for example, both niningerite and keilite in EH chondrites belong to the same continuous solid-solution series without a phase boundary or a miscibility gap in between and that they have the same Na-chloride type structure. More details of this particular topic are published by Skinner and Luce (1971).

Superficial evaluation of the habit of schreibersite associated in different assemblages may induce a pitfall, thus masking its diverse formational mechanisms recorded during the various succeeding evolutionary stages of the same meteorite. The reliance on only one habit and ignoring the others in the same meteorite that emerged from timely and genetically different episodes is an unrealistic generalization. Schreibersite is present in metal nodules as shapeless grains, but never as prismatic tetragonal prisms (rhabdite). Such rhabdite habit emerges only when this phosphide crystallizes from a P-bearing metal liquid (Buchwald 1975). However, it is present as spherical monomineralic inclusions in oldhamite, niningerite, keilite, and troilite in metal-sulfide nodules and matrices of EH and in sulfide-rich matrices in EL chondrites (El Goresy et al. 1988; Lin and El Goresy 2002) for example also in MS-17 and MS-177 but as shapeless objects in metal nodules. The schreibersite spheres in oldhamite and other sulfides might have been enclosed from a swarm of spherical phosphides in the nucleating host sulfides from the specific region from which they emerged. It is then unrealistic to solely cling to the spherical form of schreibersite confined to matrix sulfides and declare it as "clear evidence" for melting of the chondrite as a whole. Schreibersite patches inside metal nodules do not have the same habit and formational mechanism as those inside matrix sulfides.

Also of special importance is to investigate the habit and nature of carbon species, the assemblage in which they individually nucleated and grew, their abundances and location in the different lithologies of the same EC, their association, growth sequence in the various assemblages, their carbon isotopic compositions in the different lithologic units of the same meteorite, and specifically their N-isotopic compositions in comparison to that of the coexisting sinoite (Si_2N_2O) in EL3. Unfortunately, these genetically important details were not recognized or were entirely ignored in several previous studies (e.g., Humayun et al. 2009; Bischoff et al. 2010; Van Niekerk and Keil 2011; Horstmann et al. 2014) to the stage to declare that "any graphite in an EL-chondrite" regardless of its habit and the lithology in which it occurs is claimed to have exsolved from FeNi metal during taenite-kamacite inversion upon cooling. Last but not least, in situ fine-scale investigation of short-lived isotopic systems like $^{36}Cl/^{36}S*$ in lawrencite or sodalite, $^{53}Mn/^{53}Cr*$ in manganoan sphalerite, or alabandite using SIMS or NanoSIMS, is required which could deliver important details on the earliest stages of their formation (El Goresy et al. 1992; Lin et al. 2011).

Origin and formational mechanism of sinoite first encountered in an equilibrated EL4 chondrite by Andersen et al. (1964) and later in EL6 members (Rubin et al. 1997) appear to be so far unconstrained. The originally proposed mechanism envisages reaction of N_2 gas allegedly stored and then claimed to have been released from hypothetical crystal defects in troilite with a SiO_2 polymorph and Si alloyed in kamacite (Rubin et al. 1997), alternatively, by shock melting of unknown precursors (Rubin et al. 1997). None of the sinoite-bearing assemblages in equilibrated EL chondrites show any support for either melting mechanism since kamacite and silica in these chondrites do not depict any textural evidence for replacement of kamacite at its boundaries by sinoite. In contrast, recently, large idiomorphic stubby and prismatic sinoite crystals were first discovered in fragment MS-17 from the Almahata Sitta $2008TC_3$ asteroid (Lin et al. 2011) and suggested to be solar condensates from a gas with C/O ratio >1. This report not only casts considerable doubt on the previously proposed origin but also calls for careful documentation of the various sinoite-bearing assemblages in EL3 chondrites in meteorite falls.

Also of high importance is the partitioning behavior of refractory siderophile trace elements as a function of the carbon and silicon contents of the FeNi metal (e.g., Chabot et al. 2008, 2010; and references therein) and if the metal declared so far as standard kamacite is indeed carbon-free kamacite? And specifically if its textures reveal unequivocal evidence for its formational mechanism by melting or agglomeration as cold accreted conglomerate dominated by metal micropebbles? This parameter, provided that if based on meticulous petrographic characterization of many

individual metal nodules, their constituents, and critically applied, may reveal additional important information on the possible origin of metal. In evaluating the above spelled out prerequisites for a meaningful procedure, the most crucial step always remains a detailed meticulous petrographic database clarifying the nature and textures of the different metal constituents.

The inventory of refractory siderophile elements (Re, Os, W, Ir, Ru, Mo, Pt, Rh, V, Ni, Co, Pd, Fe, and Au) was a subject of experimental investigations as a function of S-, C-, Si-contents, and melting (Campbell et al. 2003; Chabot et al. 2006, 2008, 2010; and references therein). The partitioning coefficients of the refractory siderophile elements in metal between the solid metal and the carbon-bearing metal melt increase upon increase of the C-contents of the metal melt (Chabot et al. [2008] and references therein). A meaningful evaluation of the refractory siderophile inventory if resulted from condensation at 1500 K, below 1470 K, involving melting of the metal basically requires determination of the carbon content and other light elements (C, P, Si, and S) of meteoritic metal (Okamoto 1990; Campbell et al. 2003; Chabot et al. 2008, 2010). Surprisingly, this crucial analytical prerequisite was never conducted in any metal studies in EH3 or EL3 chondrites (Humayun et al. 2009; Bischoff et al. 2010; Van Niekerk and Keil 2011; Horstmann et al. 2014), and the results showing depletions in the most refractory siderophiles were automatically declared to be "indicative" of dynamic metal melting (e.g., Humayun et al. 2009; Bischoff et al. 2010). Condensation calculations and the refractory siderophile household in metals in CAIs measured by LA-ICPMS deliver convincing evidence for a flat pattern of refractory siderophiles if condensed at or below 1470 K (see fig. 10b in Campbell et al. 2003). In contrast, Humayun et al. (2009) declare that "new siderophile element data confirm that metal-kamacite associations in EL3s represent injected impact melts." This is a conclusion that lacks any supporting textural evidence for melting and metal melt injection and is discrepant with generally accepted robust shock-induced or ambient melting parameters (McCoy et al. 1999; El Goresy et al. 2011b, 2015; Lin et al. 2011). Avoiding this pitfall also calls for determination of the C-content of the metal, NanoSIMS investigations of the minor elements inventory, and careful search for impact melting-induced high-pressure phase transformations. These issues, along with others, were unfortunately entirely ignored or their relevance not recognized in many previous papers recently published on enstatite chondrites claiming "evidence for melting of the metal nodules."

RESULTS

Microscopic Investigations

Major part of the published data on ECs, except for Abee and Qingzhen EH chondrites, resulted from investigations of Antarctic and/or Northwest African finds. We consider that many of these finds are exceedingly inadequate as a result from the quite variable weathering effects due to prolonged terrestrial residence thus removing certain weathering-sensitive but geochemically important minerals and carriers of crucial cosmochemical signatures like, for example, oldhamite, which holds more than 60% of the REE chondrite budget, niningerite, keilite, and alabandite whose FeS-MgS-MnS spatial compositional variations in individual grains adjacent to troilite are of significant genetic importance for uncovering the thermal history. The EH chondrites ALHA 77296 (El Goresy, unpublished data) and EL6 Atlanta, Blithfield and Kota Kota (Ramdohr 1963, 1973) are heavily weathered leading to considerable damage of oldhamite up to removal of its major part now present as holes filled with Ca sulfate weathering products. Unfortunately, these holes were misinterpreted as resulting from impact melting and oldhamite melt migration for a few tens of centimeters (Rubin and Wasson 2011). Furthermore, removal of other sulfides in particular troilite by weathering also erases the pristine signature of the high field strength elements. Hence, our investigations on EL3, with the exception of MAC 88136, are consequently confined to falls recording minimal weathering effects. In this monograph we mainly concentrate on studies of the two Almahata Sitta EL3 meteorite fragments MS-17 and MS-177 emerged from the asteroid 2008 TC_3 (see also report by Lin et al. [2011] and preliminary report by Bischoff et al. [2010]). MS-17 was originally assigned an equilibration grade as EL3/4 with claimed impact-melt metal pockets (Bischoff et al. 2010). Our investigations reclassify this primitive stone to EL3 and in addition convincingly negate "impact melting of FeNi metal and metal melt migration in preexisting voids in regolith of parental asteroids or pre-accretionary melting." Horstmann et al. (2014) meanwhile negated the validity of their previous unconstrained assignment of the impact melting of metal also previously claimed by Bischoff et al. (2010).

MS-17 and MS-177 fragments were vacuum impregnated by Crystal Bond 509 prior to sectioning in individual slices with a wire saw in order to hermetically seal off open fractures and voids, hinder removal of important mineral constituents, and prevent contamination from polishing material like SiC or diamond from grinding and polishing pastes and

powders. Sections were highly polished with 0.25 μm diamond with ethanol as a polishing medium. They were then systematically investigated in reflected and transmitted light at the Leitz Orthoplan optical microscope for comprehensive petrography and to select assemblages for detailed documentation with a laser microRaman spectroscopy, field-emission-scanning-electron microscopy (FESEM), electron microprobe techniques (EPMA), LA-ICPMS trace element investigations, and NanoSIMS 50L isotopic analyses.

Petrography

Both EL3 MS-17 and MS-177 asteroid fragments are individual complex trichotomous conglomerates each with distinct lithologies (1) a crowded chondrule-dominated portion seldom enclosing individual angular metal fragments but surrounded by (2) individual polygonal silicate-rich fragments dominated by a wickerwork of enstatite prisms with minor ragged FeNi metal objects, and (3) well defined round or oblong FeNi metal-rich nodules in the interstices (Fig. 1). Crowded chondrules and individual polygonal silicate-rich fragments dominate the major part of both MS-17 and MS-177 (Figs. 1 and 2). Texture and grain-size of enstatite prisms in chondrules and in the polygonal silicate fragments may superficially appear to be identical and suggest that they are chondrule fragments. However, chondrule enstatite is in its majority idiomorphic prisms enclosed in oldhamite (Fig. 1b). In comparison, idiomorphic enstatite crystals in the silicate fragments are surrounded by rings of individual chains of small oldhamite crystals (Fig. 2b). This feature convincingly morphologically sifts fragments of chondrule enstatite from enstatite in polygonal silicate-rich fragments. The metal nodules are enclosed in the interstices between chondrules, chondrule fragments, and the polygonal silicate-rich objects (Fig. 1a). Each nodule and chondrule is usually decorated by a monolayer belt of troilite-dominated fluffy sulfide-metal assemblage. The polygonal silicate-rich objects are barren of such sulfide belts. Presumably, they were formed after the accretion of the troilite-dominated fluffy belts around chondrules and metal nodules but prior to the bulk accretion of all three lithologies. Antarctic MAC 88136 in principle depicts similar trichotomous lithologies as well. The nature of the metal nodules in Antarctic EL3 chondrites was not recognized before in previous papers and the metal nodules were unrealistically assigned therein as impact melts or pre-accretionary melt pockets, respectively (Humayun et al. 2009; Horstmann et al. 2014; and references therein).

Chondritic Lithology

These lithologies are dominated by unsorted chondrules and their fragments with sizes of intact chondrules of up to 4 mm. Mineral constituents in chondrules are oldhamite, enstatite, diopside, and rarely forsterite. Several chondrules occasionally contain inclusions of angular metal fragments. Yet, chondrules are generally characterized by very low FeNi metal abundance. A novel finding in EL3 chondrites is the observation that individual chondrules contain graphite books in the cores and/or are covered by single idiomorphic graphite books ranging between 50 and 70 μm in size (Fig. 3). This specific association of graphite books with chondrules was not recognized in many previous publications on ECs but graphite books in EH5 were claimed to be of igneous origin (Rubin 1985). Graphite books are also present as clusters between chondrule fragments and the polygonal silicate objects. We will adequately address the suggested igneous origin of graphite books in the discussion section below. The REE inventory of numerous oldhamite grains was measured by LA-ICPMS and is reported in the trace element section. Carbon and nitrogen isotopic compositions of graphite morphologies in the different lithologies in MS-17 and MS-177 were measured by NanoSIMS 50L and the results are given in the NanoSIMS analyses section. Each chondrule is covered with a fluffy belt of troilite-metal assemblage (Fig. 1a) with well-separated individual idiomorphic troilite crystallites thus advocating for accretion in a nonturbulent medium prior to assembly of the chondrules together. Broken surfaces of chondrules are barren of such sulfide belts attesting that the belt decoration took place prior to chondrule fragmentation. The texture negates any melting episode or violent mechanism during or after deposition of metal-sulfide assemblage belts covering the individual chondrules and the subsequent accretion of chondrules, polygonal silicate wickerwork objects, and metal nodules. This is also evidenced by the lack of any eutectic-like metal-troilite texture.

Polygonal Coarse-Grained Silicate Fragments

These objects generally classified in the majority of previous publications as matrix silicates are, however, distinct from the metal nodules in both EH3 and EL3 in that they are regularly dominated by idiomorphic coarse-grained enstatite crystals with minor diopside and forsteritic olivine and diminishing contents of FeNi metal inclusions. Their outlines feign some similarities to chondrule fragments and hence could be mistaken as such. An important compositional feature helping to distinguish them from chondrule fragments is the

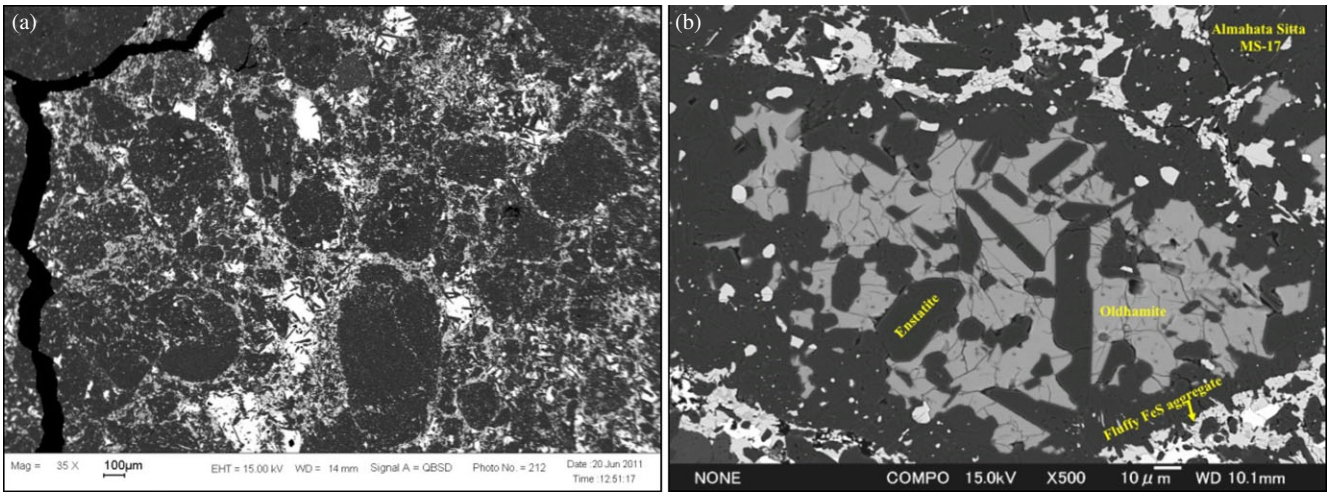

Fig. 1. a) A BSE-SEM photograph general view section No. 1 of fragment MS-177 depicting abundant chondrules, few polygonal silicate fragments, and several metal nodules (white). b) A single oldhamite crystal occupies up to 70% of the chondrule. Enstatite occurs as idiomorphic prisms enclosed in oldhamite. Notice the fluffy metal-sulfide rims at the lower left, lower right, and upper side of the chondrule. (Color figure can be viewed at wileyonlinelibrary.com.)

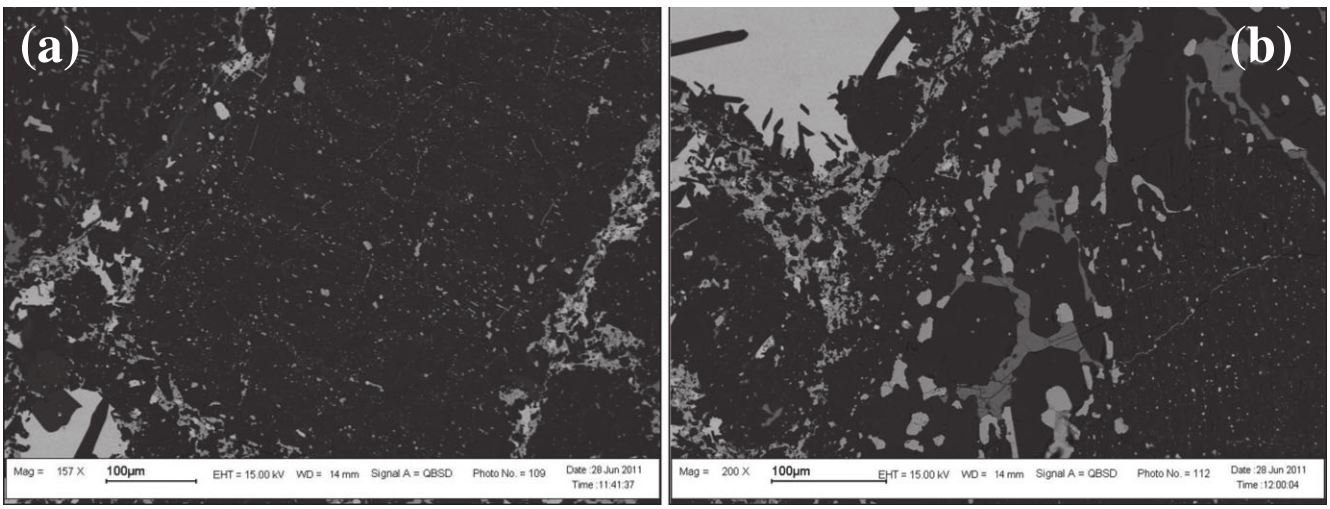

Fig. 2. a) A SEM-BSE photograph of a polygonal silicate fragment with low concentration in sulfides and metal. b) A detail from a polygonal silicate fragment from MS-17 section No. 1 depicting chains of oldhamite crystallites (gray) surrounding individual enstatite crystals. The fragment is sprinkled by individual idiomorphic troilite crystals (white).

diminishing amount and the different crystal habit of oldhamite which in these objects partially surrounds enstatite crystals (Fig. 2b) in comparison to the coarse-grained individual oldhamite crystals enclosing several idiomorphic enstatite crystals in chondrules. A detailed characterization of this lithology will be addressed elsewhere.

FeNi Metal Nodules

These are spherical and oblong objects consisting of heterogeneous conglomerates of numerous FeNi metal-rich objects hereafter designated as metal pebbles. Contrary to previous reports (Bischoff et al. 2010; Horstmann et al. 2014; and some references therein) we find no evidence for shock-induced melting of the metal nodules. Remarkably, in contrast, we encounter a menagerie of mineral constituents of variable grain-sizes, and textures evidencing their primitive nature and variable assemblages (see also El Goresy et al. [1988] for comparison with different nodule types in EH3 chondrites). Metal nodules in EH3 contain a collection of sulfides, in high abundance: Ti-troilite, niningerite (or keilite), daubréelite, djerfisherite, caswellsilverite

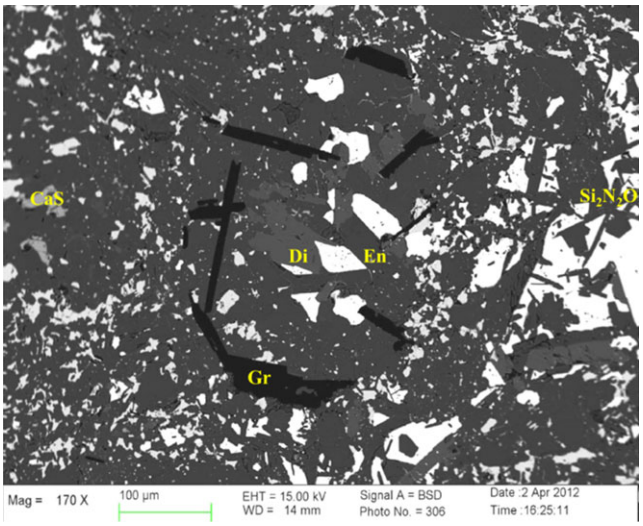

Fig. 3. An oval enstatite-diopside chondrule from MS-177 overgrown by idiomorphic graphite books. The chondrule also contains few graphite books inside. (Color figure can be viewed at wileyonlinelibrary.com.)

($NaCrS_2$), Si-bearing kamacite, perryite in addition to schreibersite, enstatite, and occasionally graphite (fig. 3 in El Goresy et al. 1988). Here, kamacite is present as oval or polygonal clasts whereby each kamacite clast is entirely decorated with submicron-sized silicates around all its surfaces (see Fig. 12). Remarkably, sulfide and schreibersite fragments are barren of such silicate decoration attesting that they escaped the decoration episode in EH3. In addition, troilite grains depict triple junctions indicating thermal annealing thus sintering metal clasts and sulfide fragments together but with no evidence of melting.

Metal nodules in MS-17 and MS-177 are in comparison multicomponent metal-dominated objects enclosing idiomorphic sinoite with various habits from prisms to stubby crystals; feathery fan-shaped graphite grown on and encapsulating sinoite crystals or their fragments; enstatite and diopside prisms, with inclusions of shapeless schreibersite; minor fractured cohenite; and lawrencite but all these constituents together aggregated and compacted in a matrix of a metal conglomerate (Figs. 4–7). All 43 metal nodules studied in this monograph consist of major heterogeneous FeNi metal alloys, with inclusions of shapeless schreibersite, fractured cohenite, oldhamite, sinoite, enstatite, minor diopside, small idiomorphic troilite crystallites, and fan-shaped feathery graphite. Enclosed mineral assemblages characterize four nodule types. Metal nodules are dominated by crowded concentrically zoned metal pebbles (Fig. 4a). Careful screening at high magnification and high contrast BSE-SEM disclosed important details of mineral constituents and their texture. Surfaces of individual metal pebbles are abundantly decorated with a monolayer of fine-grained sinoite (Fig. 4b). Numerous pebbles depict such decoration also in their interior nuclei thus suggesting multiple decoration episodes between growth of metal layers, sinoite decoration, and pebble agglomeration to metal nodules. Troilite crystallites inside the nodules are also occasionally decorated with sinoite crystallites. Feathery graphite does not depict such decoration.

In reflected light microscopy we identified the following four metal-rich nodule types:

1. Nodules dominated in their interior by large stubby crystals and prisms of sinoite up to 50 µm in size and minor enstatite prisms (Fig. 4b). This type is more abundant in MS-177 than MS-17.
2. Metal nodules with inclusions of idiomorphic prismatic sinoite crystals that in turn entirely enclose rounded oldhamite fragments thus attesting the nucleation and growth sequence oldhamite⇒sinoite prisms.
3. Metal nodules containing wickerwork, hereafter called "*Geflecht*" of idiomorphic, loosely touching, prismatic sinoite (Fig. 5). Prismatic sinoite is also present as a subordinate constituent mainly overgrown on the stubby sinoite crystals in the metal nodules type 1. Texture indicates that prismatic sinoite formed in the same episode but subsequent to the stubby crystals and prior to enclosure by the metal conglomerate. These nodules also contain lawrencite ($FeCl_2$) and fanning feathery graphite. These graphite fans always overgrew sinoite crystals or their fragments and are not in contact with any taenite thus negating their formation during taenite-kamacite inversion.
4. Nodules enclosing crystallographically controlled epitactic or topotactic intergrowth of oldhamite and sinoite encapsulated in enstatite and/or diopside (Fig. 6).

All the metal nodules in MS-17 and MS-177 are not homogeneous individual kamacite per se. They consist of a heterogeneous conglomerate of individual small metal pebbles of variable sizes between 10 and 25 µm whereby each pebble consists of multizoned concentric metal layers with different brightness in BSE suggestive of variable concentrations of light elements in the different metal layers (Fig. 4a) or show an interior metal pebble nucleus occasionally decorated by micron-sized sinoite crystallites that is surrounded by metal shells several of which are also individually decorated by sinoite crystallites (Fig. 4b). Remarkably, the interiors of many metal pebbles show lower brightness in BSE than the surrounding layers strongly suggesting higher concentration of a light element presumably carbon (Fig. 4a). The individual metal nodules

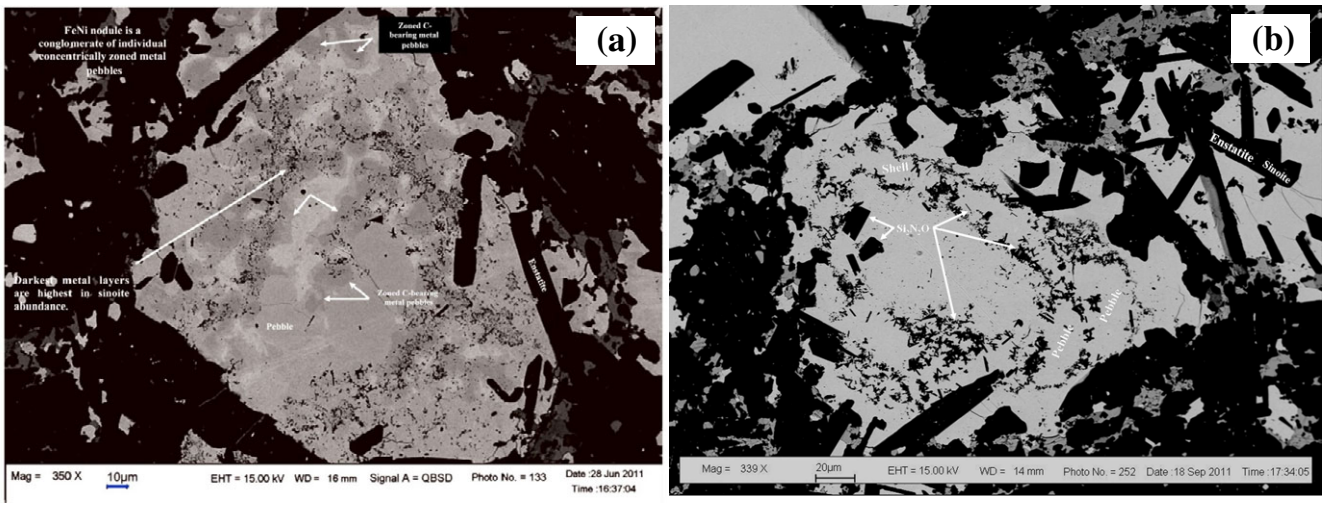

Fig. 4. a) A BSE–SEM photograph of metal nodule No. 17 in EL3 MS-17 fragment depicting the heterogeneous conglomerate of concentrically zoned metal pebbles. Cores of pebbles depict lower brightness due to higher C-content (arrows). These portions are also crowded with submicron crystallites of sinoite. b) A SEM-BSE photograph of nodule No. 34 in EL3 fragment MS-17. Nodule has a core encompassing numerous sinoite-decorated micropebbles with two large idiomorphic sinoite (Si_2N_2O) stubby crystals and is decorated by submicron crystallites of sinoite (white arrows). The core is covered by several metal pebbles and a metal shell. (Color figure can be viewed at wileyonlinelibrary.com.)

occasionally enclose crowded nests of gently touching prismatic sinoite crystallites (Fig. 5). Many pebbles are also decorated on their nuclei and exterior surfaces with micron-sized sinoite grains. A large number of metal nodules enclose fractured cohenite, feathery fan-shaped graphite, and submicron-sized sinoite. Kamacite-cohenite dendritic texture were not encountered in any of the 43 metal nodules investigated. Every metal nodule is surrounded by a fluffy sulfide-metal belt consisting of major idiomorphic troilite single crystallites, minor alabandite, and FeNi metal fragments. In comparison to graphite books in the chondritic lithology in MS-177 (Fig. 3), feathery graphite in nodules in MS-17 consist of small platelets 2–5 μm in size attached together like fluffy fanning branches (Figs. 5b, 8–11). The platelets are always nucleated either on sinoite crystals, on their fragments, or other graphite platelets thus indicating that graphite feathers nucleated as platelets and grew first subsequent to stubby sinoite fragmentation and used them as nucleation sites.

The above described nodule types may not entirely reflect all existing varieties of metal nodules present but document the diversities and complexity of the genetic processes that led to their formation and assembly. The encountered complex texture of the metal nodules is not in fact novel but already recognized by Lin et al. (2011) in fragment MS-17 from the Almahata Sitta asteroid. They were not reported before from any Antarctic or Saharan EL3 chondrite albeit remarkably not recognized by others in Almahata Sitta EL or EH chondrites (Bischoff et al. 2010; Horstmann and Bischoff 2014). It is worthwhile to recall that PGE-bearing metal Fremdlinge in CV3 chondrites are also multiobject constituents that contain inclusions interpreted either to have condensed at different temperatures or originated from different sources in the nebula without any evidence of melting (Campbell et al. 2003).

The variability of the mineral constituents in the different metal nodules and the multiple oldhamite-sinoite growth relationships offer a possibility to critically test the different formational mechanisms of the metal nodules proposed and individually the different lithologies. Furthermore, abundance, habit, and texture of sinoite are remarkable. Many metal nodules enclose mainly large idiomorphic stubby ≥ 50 μm or prismatic sinoite crystals (Figs. 4–5), some with polysynthetic lamellar twinning (not shown here) and prismatic enstatite in the nodules interior. Many metal pebbles therein are decorated by fine-grained sinoite crystallites on their surfaces attesting accretion after their individual decoration (Fig. 4). Encounter of the various sinoite assemblages is also novel in EL3 chondrites and the diversity recognized here (Figs. 4–6) is exceptionally remarkable attesting a complex genetic evolution in their source region addressed below.

The topotaxial intergrowth of prismatic sinoite with an oldhamite crystal enclosed in diopside (Fig. 6) indicates crystallographically controlled simultaneous nucleation and growth of both oldhamite and sinoite thus predating their joint enclosure in the host diopside.

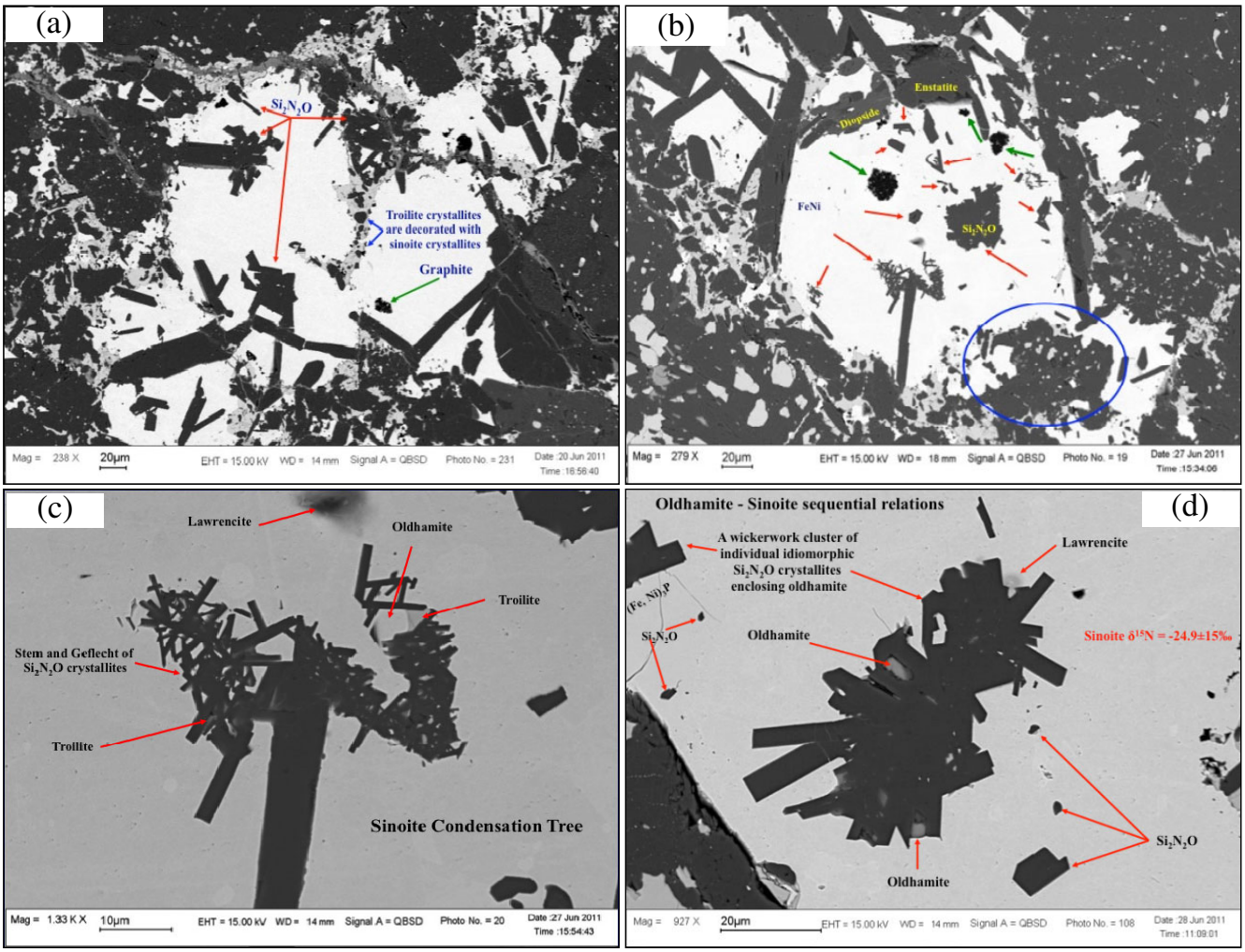

Fig. 5. a) A BSE-SEM photograph of a round metal nodule in MS-17 enclosing several sinoite intergrowths (red arrows), troilite multigrain (blue arrows), sinoite crystallites, and fluffy graphite (green arrow). b) A metal nodule with high abundance of sinoite intergrowths Geflecht (red arrows), feathery graphite (green arrows). Blue encircled object is a polygonal silicate fragment. c) A detail from the lower side of (b) depicting a typical fluffy sinoite Geflecht with few troilite inclusions between the sinoite prisms. Notice the lawrencite inclusion in the metal at the upper edge of the figure. d) A high-magnification photograph of a metal nodule from MS-17 depicting a wickerwork of prismatic sinoite crystals with several oldhamite inclusions in sinoite. N-isotopic composition of sinoite ($\delta^{15}N = -24.9 \pm 15‰$) was measured on individual sinoite prisms in this Geflecht. (Color figure can be viewed at wileyonlinelibrary.com.)

This intergrowth attests detail in the sequence oldhamite + sinoite ⇒ enstatite and/or ⇒ diopside. This texture also presents convincing evidence against any melting and quenching mechanisms. It is worthwhile to emphasize that sinoite amorphizes by dynamic events as experimentally demonstrated by Sekine et al. (2006). In addition, several adjacent prismatic diopside and enstatite crystals in this metal nodule contain numerous idiomorphic sinoite crystallites as well as reworked or considerably consumed sinoite residues (Fig. 7). The texture is strongly suggestive of incorporation of idiomorphic sinoite in the nucleating and growing pyroxenes. This texture is reminiscent of the sequence of the mechanism predicted by Fedkin and Grossman (2006) and Grossman et al. (2008), respectively, that "enstatite condensing in the nebula at $P = 10^{-4}$ bar would nucleate and consume pre-existing sinoite condensates below 1100 K." It remains to be shown if enstatite or diopside emerged through consumption of sinoite would also inherit cosmochemical signatures of sinoite in enstatite and in the chondritic lithology.

Furthermore, the assemblages and their textures point to distinct nucleation and growth mechanisms in two distinct sequences in different metal nodules involving oldhamite, sinoite, enstatite, diopside, and feathery graphite, thus manifesting different growth sequences (see next chapter). We encounter the following assemblages:

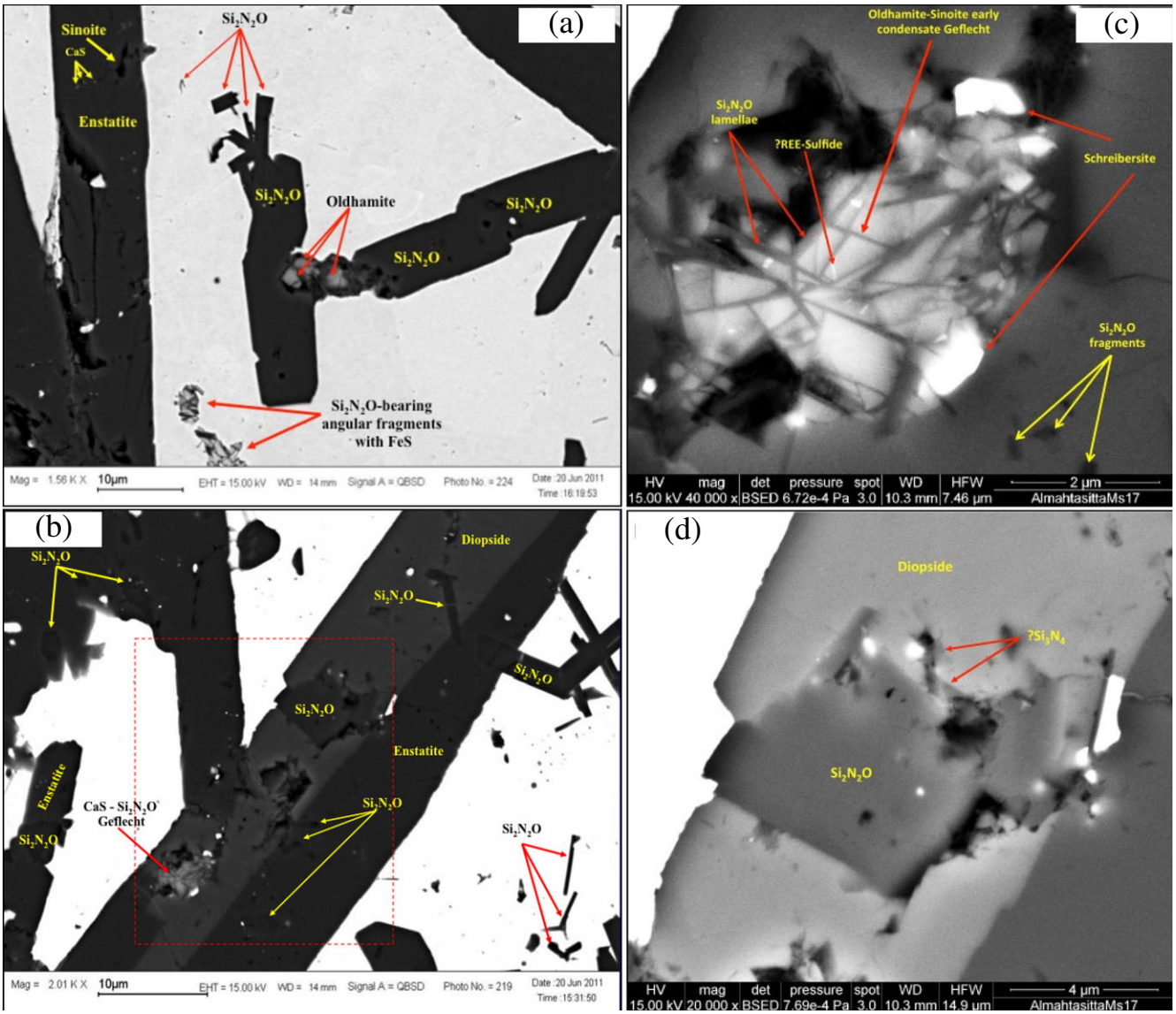

Fig. 6. a) A high-magnification BSE-SEM photograph showing in the lower left angular fragments of fine-grained troilite-sinoite intergrowth. Sinoite idiomorphic prisms with inclusions of oldhamite (red arrows). On the left side enstatite prisms with sinoite inclusions. b) An assemblage of enstatite and diopside enclosing idiomorphic sinoite prisms and a wedge-shaped basal section of sinoite. Diopside encloses a topotaxial intergrowth of oldhamite and sinoite lamellae whose details are shown in (g) below. Red dotted frame marks the area scanned by NanoSIMS 50L. c) A high magnification of the central portion of (b) depicting in detail the topotaxial intergrowth of oldhamite and sinoite lamellae in (b) and reworked sinoite fragments (yellow arrows) in diopside. d) Detail from (b) showing the wedge-shaped basal section of the idiomorphic inclusion of a sinoite prism in diopside evidencing sinoite nucleation and growth prior to the formation of both pyroxenes. Notice the small inclusions of possible nierite (Si_3N_4). (Color figure can be viewed at wileyonlinelibrary.com.)

1. Idiomorphic sinoite prisms entirely enclosing reworked oldhamite grains (Fig. 5d)
2. Enstatite and diopside prisms enclosing idiomorphic sinoite crystals which in turn enclose oldhamite residual fragments (Fig. 6a)
3. Fragments of sinoite crystals with residual small oldhamite inclusions, whereas the sinoite fragments are tightly overgrown or encapsulated by feathery graphite (e.g., Fig. 10).

The intimate intergrowths with the two textural varieties of the assemblage oldhamite-sinoite-enstatite and feathery graphite found in FeNi nodules were not encountered in the chondritic lithology and the polygonal silicate fragments. They were not previously reported from any Antarctic or Saharan EL3 chondrite find. The oldhamite-sinoite-feathery graphite texture (Fig. 10) is strongly suggestive of increase in the C/O ratio in the source medium after fragmentation of

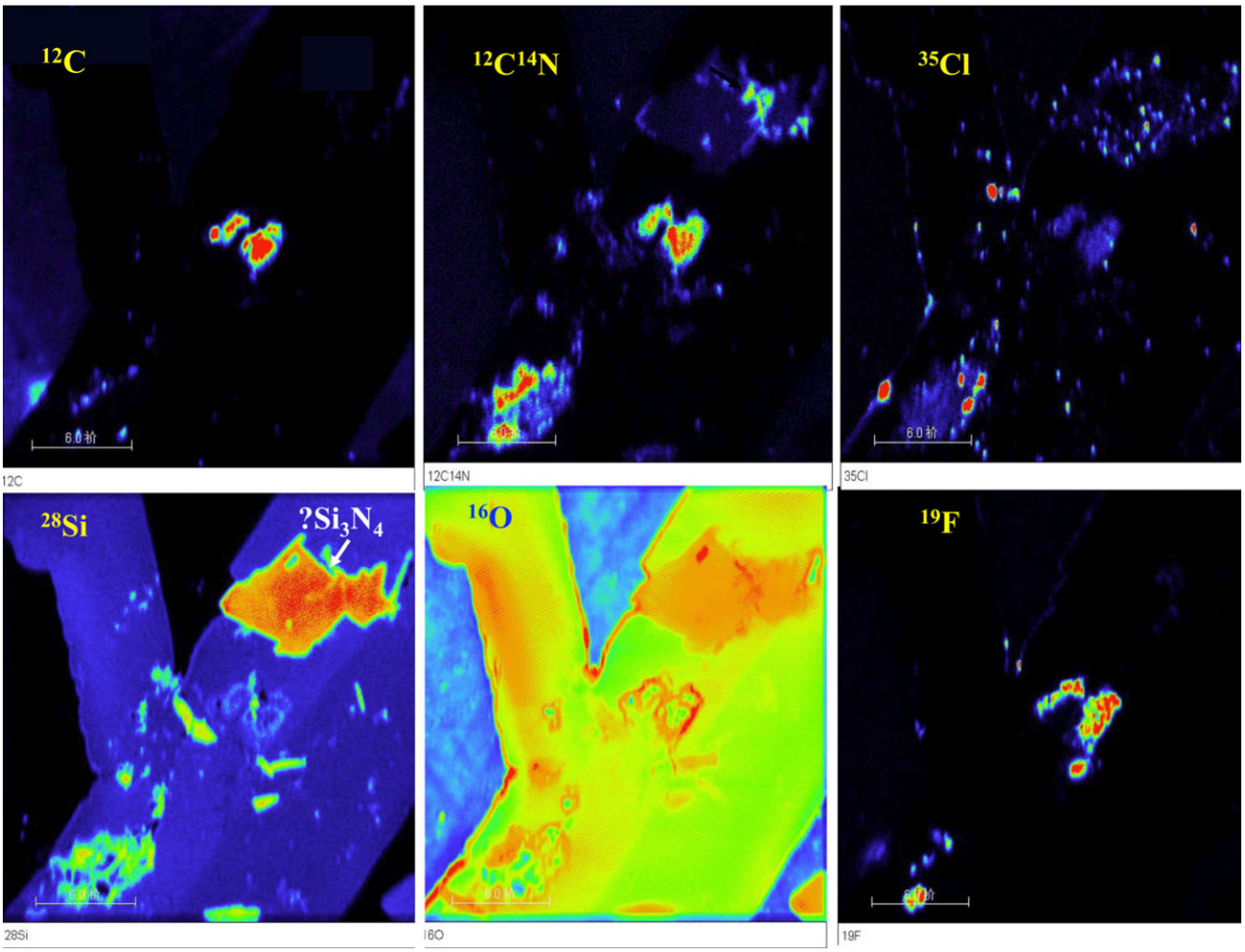

Fig. 7. Elemental map for ^{12}C, $^{12}C^{14}N$, ^{35}Cl, ^{28}Si, ^{16}O, and ^{19}F photographed at NanoSIMS 50L. The ^{28}Si and ^{16}O maps exactly show the texture and location of sinoite inclusions and their progressively consumed residues inside enstatite and diopside, respectively, of Fig. 6b. Ion maps for ^{12}C and $^{12}C^{14}N$ highlight the locations of graphite inclusions in pyroxenes. ^{35}Cl map locates lawrencite as a halogen carrier phase. (Color figure can be viewed at wileyonlinelibrary.com.)

originally idiomorphic sinoite thus inducing nucleation and growth of feathery graphite around the idiomorphic sinoite crystals and their fragments. We conducted systematic isotopic investigation of the fan-shaped feathery graphite in FeNi metal nodules and the graphite books in and around chondrules with NanoSIMS 50L to characterize their C- and N- isotopic signatures and the results are given below.

Morphologically similar FeNi metal nodules were reported in the past from Antarctic EL3 chondrites and inferred to be "shock-induced metal melt pockets" (e.g., Humayun et al. 2009) and in stark contrast in MS-17 of Almahata Sitta asteroid (Lin et al. 2011) as earliest condensates. Figure 4 presents several lines of evidence against the impact-induced or pre-accretionary melting. FeNi nodules contain feathery graphite consisting of a mechanical accumulate of individual very small graphite platelets <6 μm in diameter (see details in Figs. 8–10) with the platelets closely overgrown around sinoite seeds. We will show below that the graphite platelets in the same feathery graphite objects have considerably variable nitrogen concentrations. This texture is strongly suggestive that the graphite platelets originated from variable sources with different nitrogen-contents but accreted in a later episode. The chondrules in MS-177 contain in contrast exclusively graphite books (Fig. 6).

We find in the 43 studied individual metal nodules two distinct nucleation and growth sequences involving oldhamite, sinoite, enstatite, diopside, and feathery graphite: (1) The sequence oldhamite ⇒sinoite ⇒enstatite ⇒diopside and (2) oldhamite ⇒sinoite ⇒feathery graphite ⇒enstatite ⇒diopside. These two sequences were never encountered together in the same metal nodule of the 43 metal nodules here investigated.

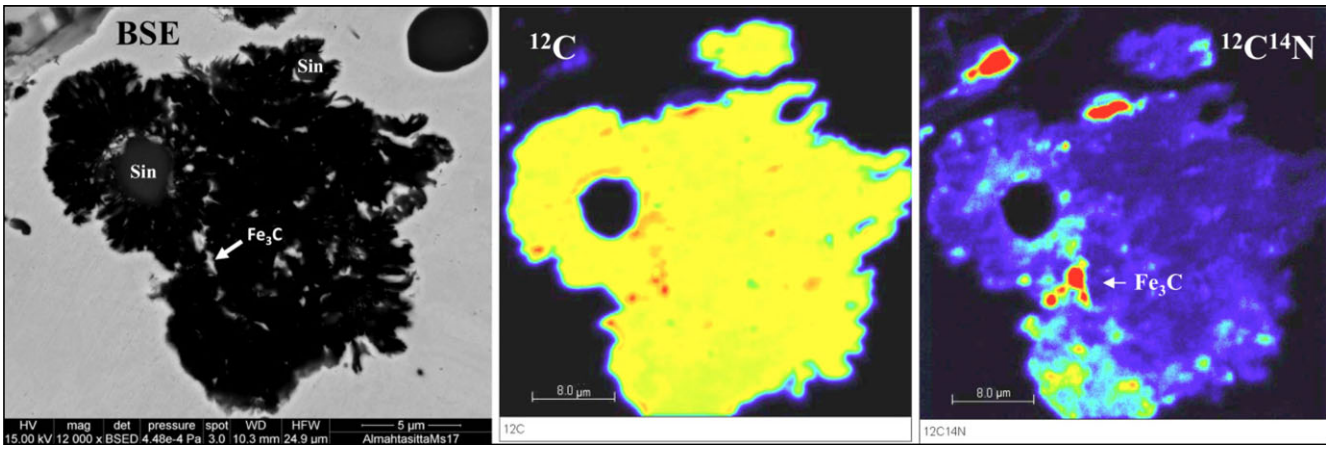

Fig. 8. Left: Rounded sinoite grains (Sin, light gray) overgrown and encapsulated by feathery graphite. Middle: ^{12}C elemental map. Right: $^{12}C^{14}N$ (Mass 26, representative of N) map depicting the heterogeneity of the ^{14}N abundance among the graphite platelets. Feathery graphite consists of individual platelets with low N-concentration (dark blue on the upper right) and platelets with higher N-content (bright blue and green lower left). (Color figure can be viewed at wileyonlinelibrary.com.)

The delicate textures involved in the sequences and lack of deformation of graphite indicate that they are not impact related but fluffy nucleated, accreted, and were then overgrown and sealed by the metal (see Figs. 7–10) which were sequestered in different FeNi metal nodules and followed in the final stage by accretion of the metal nodules conglomerate together with polygonal silicate objects and chondrules in the EL3 conglomerate. This hints to several but presumably closely related but diverse nebular sources of the metal nodule types and chondrule lithologies that need to be substantiated and the formation conditions need to be isotopically checked for (see the discussion section below).

A further important observation is the lack of any evidence for quenched immiscible melts experimentally demonstrated to be important constituents of any melting and subsequent quenching of multiphase material of enstatite chondrite parentage (McCoy et al. 1999). See discussion section below for more details.

In short, stark differences in mineralogy and texture of the three lithologies strongly hint to distinct formational conditions and episodes with high but different C/O ratios at which they individually evolved. However, the bulk chondritic composition and the identical REE signature in oldhamite present in the texturally different lithologies in the same meteorite fragment require a common parental source reservoir for them. This common source was apt to deliver on the one hand chondrules and graphite books (Fig. 3), on the other very probably subsequently angular silicate fragments and FeNi metal conglomerate the latter contains sinoite and feathery fan-shaped graphite (Figs. 8–10). The sinoite-enstatite and/or sinoite-diopside intergrowths and consumption reactions found in the metal nodules were not encountered in the chondritic lithology thus strongly supporting the notion that these two lithologies emerged at different but probably subsequent episodes. Remarkably, oldhamite in the chondritic lithology (Figs. 1b, 13a) and oldhamite in matrix (pattern not shown separately) have very similar REE patterns with a negative Eu anomaly. This hints on one hand to petrologically different formational conditions of the oldhamite in the two lithologies yet on the other hand to very similar REE signature of the source medium during the CaS nucleation in both of them. Admittedly, this is a cosmochemical puzzle and it is unclear right now as how to envisage two lithological units subsequently emerging with different mechanisms from the same cosmochemical parental source, with chemically and mineralogically different components but with strictly identical REE patterns in oldhamite in both units.

This mineral inventory not only on the one hand diagnostically sifts EC from ordinary and carbonaceous chondrites, but also on the other leads to recognition of the two distinct subgroups members, whereas alabandite is present mainly in EL.

It is noteworthy to add that cosmochemical dichotomy and complementarity is also recorded in OC and CC (Ebel et al. 2015; Palme et al. 2015).

NanoSIMS Isotopic Investigations

We systematically investigated the C- and N-isotopic compositions of petrographically selected clean graphite books in chondrules, on one hand, and the feathery graphite in FeNi metal nodules on the other with a NanoSIMS 50L to characterize their isotopic

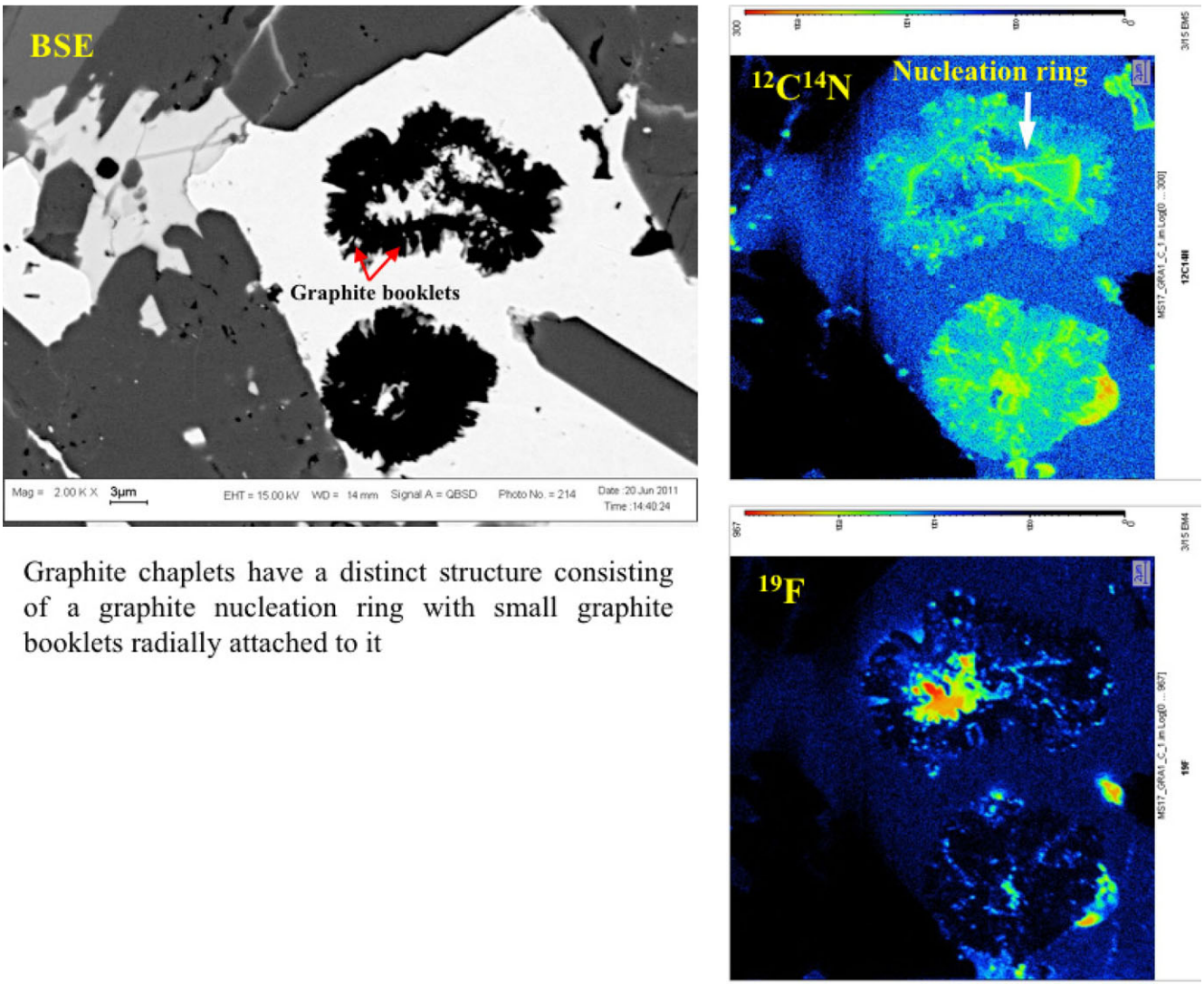

Fig. 9. Upper left: a BSE-SEM image of a metal nodule enclosing two graphite chaplets. The NanoSIMS ion map for $^{12}C^{14}N$ reveals the complexity of its structure commencing with the formation of a nucleation ring (white arrow in the upper right figure) on which individual graphite microplatelets accumulated and got somehow attached. ^{19}F map denotes locality of lawrencite the major carrier of halogens. (Color figure can be viewed at wileyonlinelibrary.com.)

signatures. We demonstrate that the combined petrographic-isotopic study indeed reveals additional so far unknown information about their origin and formational mechanisms. The oldhamite-sinoite-feathery graphite-enstatite assemblages are very promising, offering the possibility of documenting their isotopic signatures, if similar or different from graphite books in the chondritic lithology of the similar EL3 chondrite Almahata Sitta fragment MS-177. Furthermore, the difference of the growth sequence involving sinoite, graphite, and enstatite probably have resulted from change of the C/O ratio as argued before. Alternatively the difference may have emerged in different section subsource regions not with strictly solar abundances, for example, in REE but at very high and different C/O ratios (El Goresy et al. 1988, 2015; Lin and El Goresy 2002; Gannoun et al. 2011). A continuously variable C/O ratio during nucleation and growth would also call for variable concentration of carbon in solid solution in the FeNi metal nodules that need to be quantified.

MINERAL CHEMISTRY

We measured in addition to Ca and S the Mg, Mn, and Fe minor element contents of oldhamite in chondrules and matrices and tried to evaluate the genetic relevance of the minor element inventory (as MgS, MnS, and FeS) of oldhamite in an attempt to

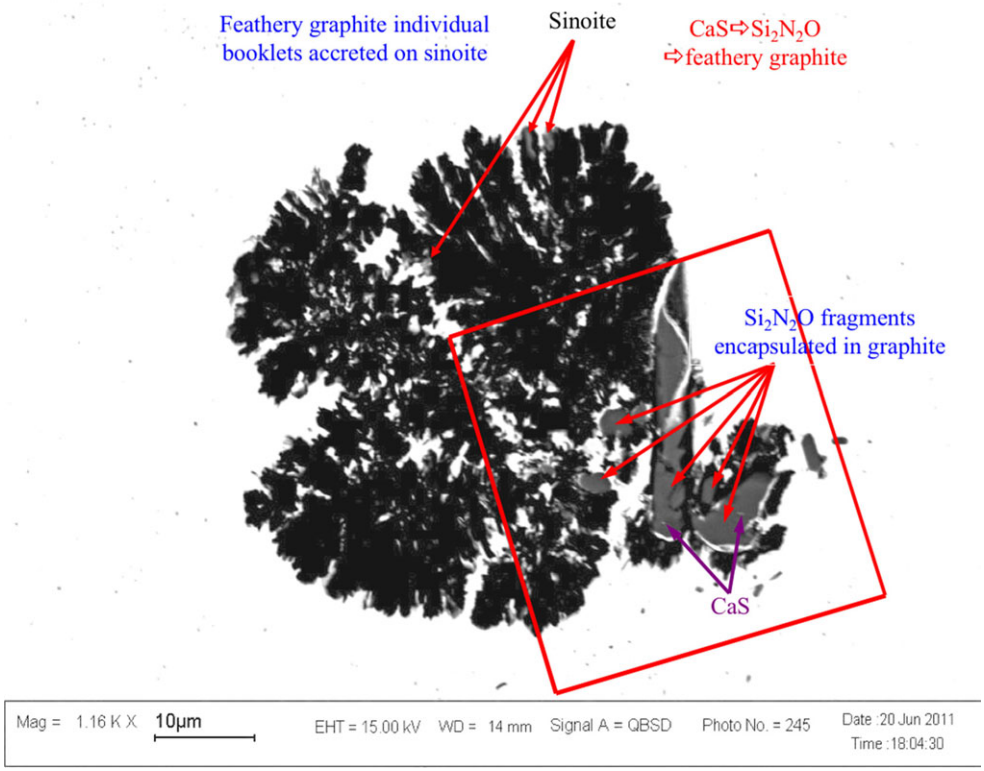

Fig. 10. Fragments of sinoite crystals with small inclusions of CaS tightly overgrown by feathery graphite fans inside a metal nodule in MS-17. Red frame outlines the area mapped by NanoSIMS 50L shown in Fig. 11. (Color figure can be viewed at wileyonlinelibrary.com.)

extract information on its temperature of formation and closure temperature of equilibration using the experimental results of the binary systems CaS-MnS, CaS-MgS, and CaS-FeS of Skinner and Luce (1971). We emphasize that such exercise with a meaningful application of the experimental results is only applicable to oldhamite grains that have mutual boundaries with each other, and those in contact with alabandite and troilite thus warranting equilibrium and interdiffusion during cooling to the closure temperature of equilibration**.** Oldhamite in chondrules is intimately intergrown with enstatite (Fig. 1b) and occasionally with diopside. Unfortunately, none of the oldhamite grains in polygonal silicate fragments (Fig. 2b) or in the metal nodules are in assemblage with alabandite, the only MgS-bearing sulfide. We were in addition confronted with the analytical problem that the extension of usually small matrix CaS crystals below the section surface is unknown. We cannot exclude that in some cases beam overlap below the section surface could have contributed to the counting rate of Mg (enstatite), Mn (alabandite), and Fe (troilite). This uncertainty required monitoring Si, Mn, and Fe counting rates and discarding results with high and unrealistic Si, Mn, or Fe counting rates. Chondrules contain large oldhamite crystals enclosing idiomorphic enstatite but neither troilite nor alabandite, thus are inadequate for such an experiment. Oldhamite in angular silicate fragments surrounds enstatite crystals but does not have any alabandite in contact (Fig. 2b). MgS-MnS and MnS-FeS ratios in oldhamite grains both in matrix and chondrules are shown in Fig. 12. Alabandite grains encountered in the sulfide belts around metal nodules and chondrules are ≤5 µm in size, hence are too small to conduct detailed EPMA analyses and specifically measure zoning profiles. Estimation of the closure temperature of equilibration of oldhamite in the matrix using the experimental data of the binary CaS-MnS requires measurements of the MnS contents in oldhamite grains directly in contact with alabandite. Such assemblage is not present in the matrix or in any metal nodule. However, we cannot entirely rule out that some oldhamite grains in the matrix are in contact with subsurface, invisible alabandite. Accordingly, our estimates of the closure temperatures of equilibration of oldhamite in the matrix are merely cautious and conservative suggestions implying that the grains were in contact and equilibrated with subsurface alabandite.

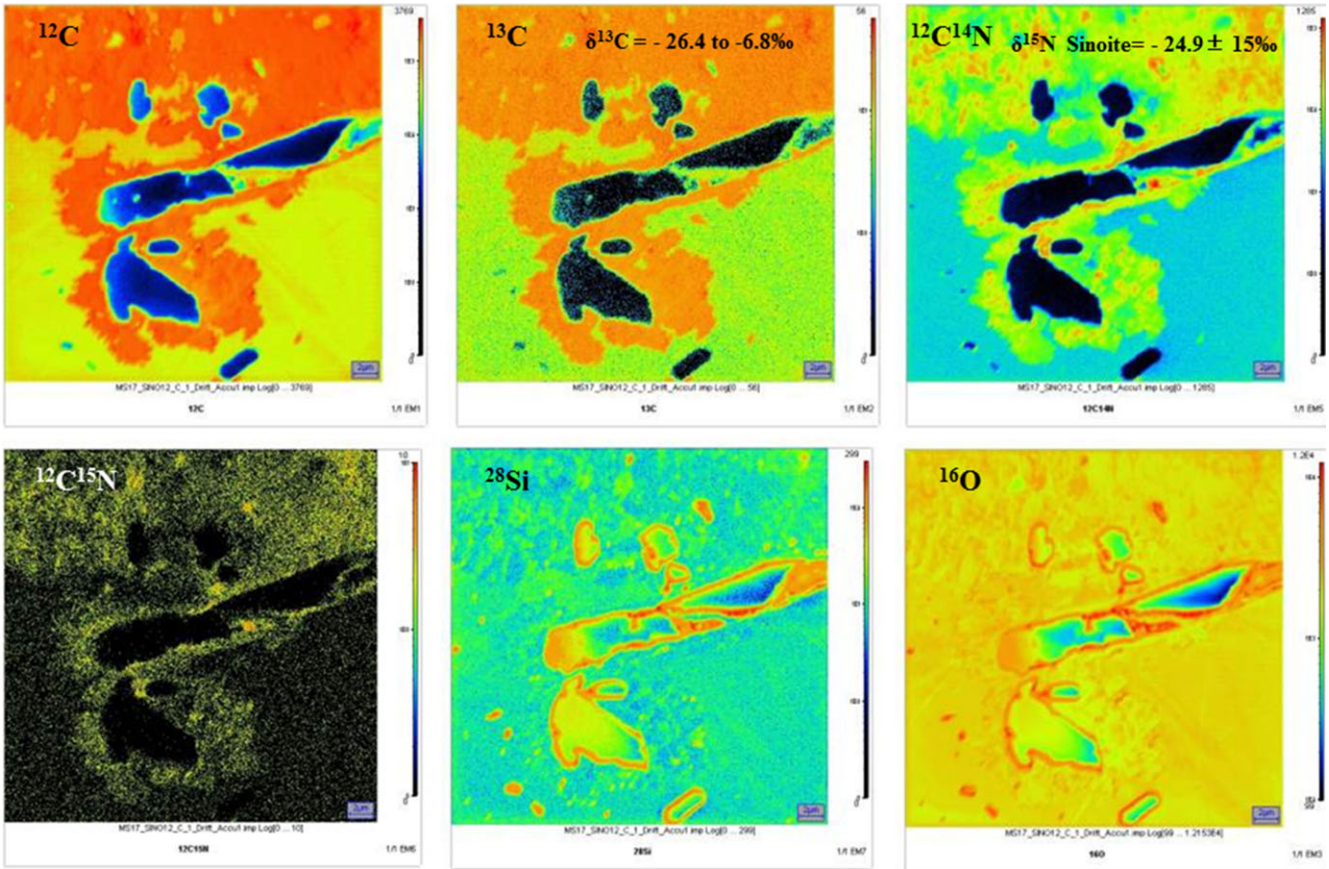

Fig. 11. Clockwise from left in upper panel elemental and isotopic ^{12}C, ^{13}C, $^{12}C^{14}N$, $^{12}C^{15}N$, ^{28}Si, and ^{16}O maps of the CaS-sinoite-graphite intergrowth shown in Fig. 10. Dark regions in the three figures in the upper panel and in the lower left are sinoite fragments. Nitrogen is heterogeneously distributed in graphite well resolved in the upper figure far right ($^{12}C^{14}N$) and the lower figure far left ($^{12}C^{15}N$). Notice the tight graphite overgrowth on sinoite well recognizable in the ^{12}C, ^{13}C, and $^{12}C^{14}N$ maps. (Color figure can be viewed at wileyonlinelibrary.com)

Oldhamite Composition

Wavelength dispersive EPMA analyses were conducted on 102 oldhamite grains. Ten analyses were discarded either due to their low total lower than 97.1 wt%, resulting from partial weathering or contamination due to suspected overlap of the electron beam on neighboring or underlying sulfides and/or silicates. Ca and S concentrations in the accepted 92 analyses varied between 53.9 wt% Ca and 42.5 wt% S (totals 98.3 wt%) and 52.8 wt% Ca and 42.5 wt% S (totals 98.1 wt%), respectively. Minor elements detected are Mn (1.25–0.93 wt%), Fe (1.3–0.35 wt%), and Mg (0.49–0.43 wt%) recalculated as MnS, FeS, and MgS, respectively. Figure 12 shows the MgS-MnS and MnS-FeS variations in the analyzed oldhamite grains both in chondrules and matrices. We refrained from including the MgS-FeS plot because it does not add any genetically important information. The plot shows the apparent dichotomous FeS concentration depicted in Fig. 12b. Figure 12a presents the MgS-MnS variations indicating a small positive slope with higher MgS contents for oldhamite higher in MnS concentrations from both lithologies. Two or three analysis points are off the trend with MgS contents more than 1.5 mole% probably due to contamination from neighboring enstatite. Figure 12b depicting the MnS-FeS variations reveals flat patterns with an apparent compositional gap in the FeS concentrations between 1.02 and 1.20 mole% thus mimicking the existence of chemically bimodal populations. FeS contents of oldhamite in chondrules and matrices plot in the two apparent populations so we suspect that this gap could eventually be a result of an analytical artifact. We hence refrained from evaluating the cosmochemical relevance of the apparent dichotomy of the FeS contents due to the considerable uncertainty about beam overlap on neighboring or underlying sulfides that may call into question the reliability of the obtained and hitherto discussed concentrations of Fe. To the first approximation and

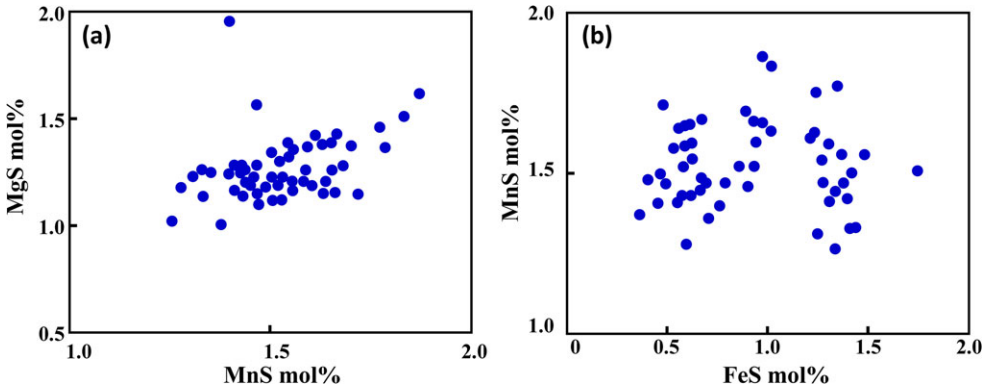

Fig. 12. a) MgS-MnS relationship in oldhamite in MS-17 and MS-177. The plot indicates a positive relationship. The two points with MgS contents higher than 1.5 mole% are probably analytical artifacts. b) MnS-FeS relationship in oldhamite in MS-17 and MS-177. The plot mimics dichotomy in the FeS concentrations both in chondrules and matrices. (Color figure can be viewed at wileyonlinelibrary.com.)

considering the above notified requirements in applying the experimental data and the precautions spelled out by Skinner and Luce (1971), we note that the low MnS contents of oldhamite might safely suggest a conservative upper limit of equilibration presumably not higher than 700 °C (see fig. 15 of Skinner and Luce 1971).

REE Patterns of Oldhamite

REE patterns of oldhamite grains both in chondrules and matrix in MS-17 EL3 fragment of Almahata Sitta asteroid (El Goresy et al. 2011a) are flat with a CI-normalized enrichment factor of ≈100 and a negative Eu anomaly (Fig. 13a). The obtained REE patterns are clearly distinct from those measured in oldhamite in EH3 chondrites. Oldhamite in EH3 chondrites depicts positive Eu and Yb anomalies (Gannoun et al. 2011) thus convincingly suggesting that the patterns obtained here have a different enrichment origin in oldhamite in EL3 MS-17 than those in oldhamite in EH3 chondrites (Gannoun et al. 2011).

Carbon Isotopic Composition of Graphite Morphologies Measured by NanoSIMS 50 L

Carbon isotopic compositions of feathery graphite fans in MS-17 and graphite books measured in MS-177, respectively, are plotted as $\delta^{13}C$ in Fig. 14. The $\delta^{13}C$ values indicate dichotomous isotopic compositions as a function of graphite morphology. Graphite books (12 analyses) in and on chondrules of MS-177 have $\delta^{13}C$ ratios of −8 to −2‰. Graphite feathers (19 analyses) in MS-17 are clearly isotopically lighter with $\delta^{13}C$ values between −26 and −6‰. In addition, the stark variation in their $\delta^{13}C$ values of the feathery graphite is consistent with lack of isotopic equilibration. This clearly negates both melting scenarios of the metal nodules by impact or melting in a pre-accretionary episode as advocated by Bischoff et al. (2010) and Horstmann et al. (2014), respectively.

DISCUSSION AND CONCLUSIONS

The research procedure applied in this investigation unambiguously demonstrates that it is indispensable to adopt a multitask research procedure mainly relying on meticulous and skillful petrographic scrutiny both at the optical microscope and SEM-BSE thus convincingly disclosing the nature, exact fabric of the encountered mineral constituents, and subsequently securing their isotopic signatures by microscale isotopic study preferably with NanoSIMS. As demonstrated, EL3 chondrites consist of complex mixtures of texturally distinct but cosmochemically complementary lithologies whose formational mechanism requires to be disentangled. Such a program calls in the first place for a critical evaluation of the reports published and cited since 1980 and earlier. A genetically important aspect that needs careful reevaluation is the widely unquestioned claim that alone "the magnitude of enrichment in moderately volatile elements in the different petrologic members in both EH and EL subgroups should reflect a reliable measure of the sequence of formation" (Kong et al. 1997). Application of this intuitive paradigm led these authors to introduce a petrologically not meaningful sequence of formation suggesting that members with higher concentrations of the moderate volatiles but of higher petrologic equilibration grade have formed earlier than any unequilibrated member with lower concentration in these elements regardless if classified in subgroup EH or

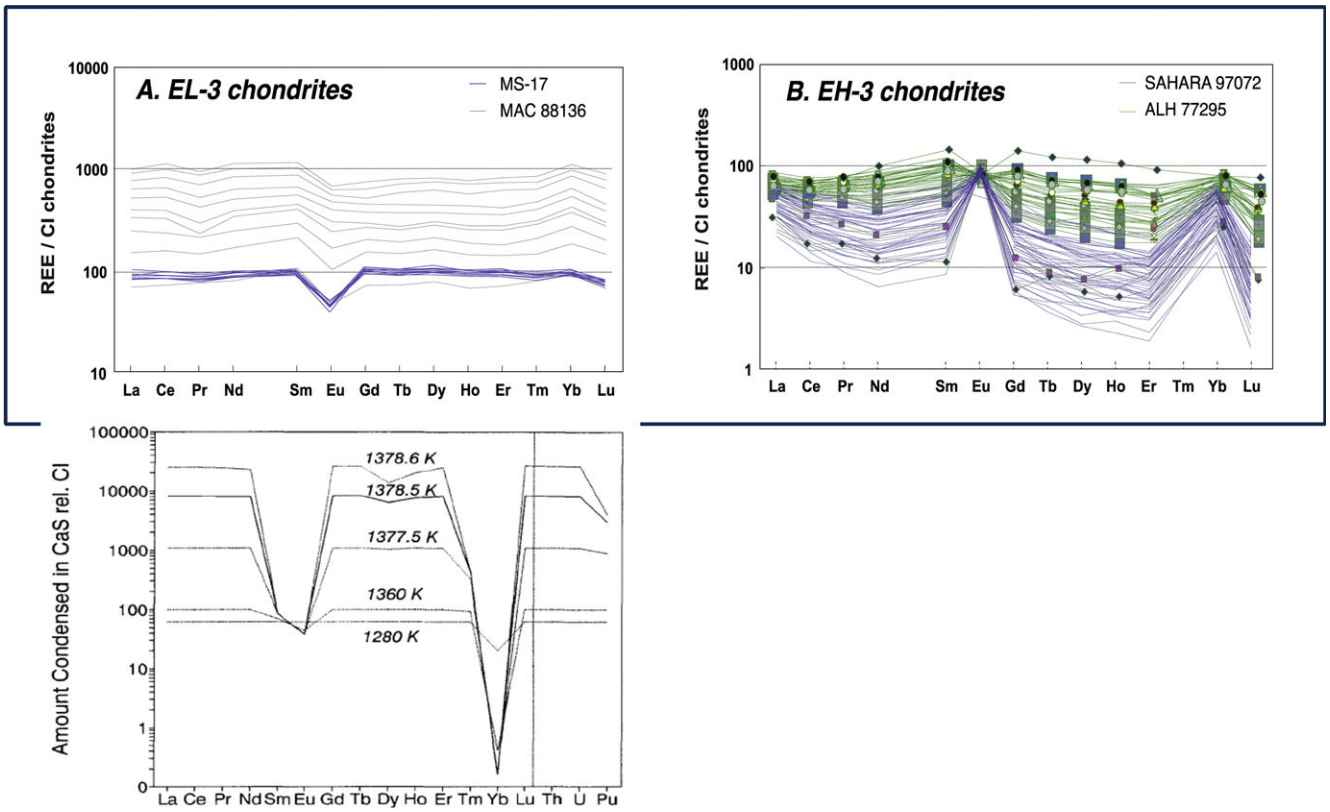

Fig. 13. Upper left is plotted the CI-normalized REE patterns of oldhamite in EL3 chondrite MS-17 and MAC 88136 indicating flat REE patterns with a negative Eu anomaly (El Goresy et al. 2011a). Upper right depict the REE patterns in oldhamite in the EH3 chondrites ALHA 77295 and Sahara 97072 with positive Eu and Yb anomalies. The lower plot depicts the CI-normalized REE patterns in oldhamite predicted as earliest condensates between 1379 K and 1280 K from a gas of solar composition (Lodders and Fegley 1993). (Color figure can be viewed at wileyonlinelibrary.com.)

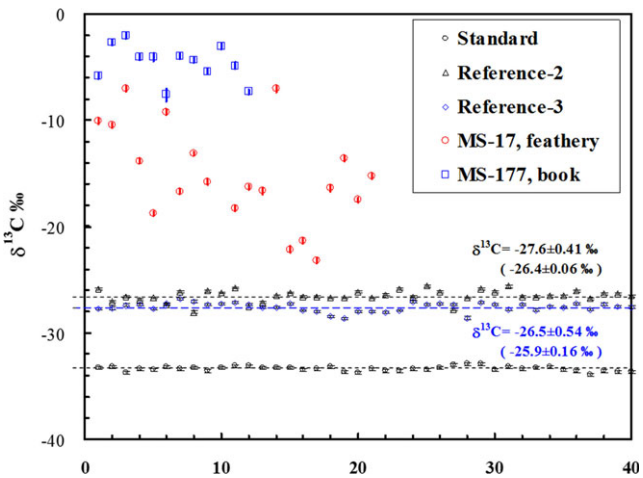

Fig. 14. A plot of $\delta^{13}C$ in feathery graphite and graphite books in EL3 fragments MS-17 and MS-177 of Almahata Sitta 2008 TC_3 asteroid. Dichotomy of the $\delta^{13}C$ is evident. Notice the heterogeneity of $\delta^{13}C$ ratios among feathery graphite in MS-17. (Color figure can be viewed at wileyonlinelibrary.com.)

EL, thus suggesting an unrealistic nebular sequence of the type EH5⇒EH3⇒EL3⇒EL6 (Kong et al. 1997). Such a sequence calls for crossover commencing with more equilibrated members then followed by unequilibrated primitive ones in the same enstatite chondrite subgroup and then further to the unequilibrated and equilibrated members of the other subgroup that have different petrology and bulk chemistry, consequently calling, for example, for the moderately equilibrated St. Marks (EH4-5) and/or Indarch (EH5) to be earlier in the sequence than the very primitive ALHA 77295 or Sahara 97072, without supporting radiometric studies of short-lived isotopic systems like $^{129}I/^{129}Xe$. We are considerably skeptical of the relevance and validity of this scheme to establish a genetically reliable sequence across EH to EL because this interpretation requires dramatic changes in bulk chemistry during their evolution also leading to reversion of the equilibration process that is, from unequilibrated to equilibrated and subsequently vice versa. This is a requirement that was never demonstrated to have played any role in any enstatite chondrite or in OC or CC either. Unfortunately, other alternatives like different parental bodies for EH and EL and even among members of the same subgroup of the enstatite chondrite clan were not considered a viable

possibility by Kong et al. (1997). We consider this proposed sequence to be unrealistic and discrepant with the petrological equilibration paradigm and findings, albeit the high quality of the bulk element inventory characterizing the individual EH or EL chondrites maintains its validity as such, for individual chondrites.

In the following paragraph we address the REE signatures of EH3 chondrites and in detail in EL3 chondrites and inventories of their carrier species. The REE patterns of bulk EH3, EL3, and their individual mineral constituents disclosed in part unexpected information. CI-normalized REE patterns of bulk individual EH3 and EL3 chondrites logically reveal on the one hand CI-normalized flat chondritic patterns (Gannoun et al. 2011; Ebel et al. 2015) thus strongly suggestive of chondrules and matrix lithologies with complementary CI-normalized bulk REE patterns. The REE patterns of oldhamite require on the other hand a critical discussion since this mineral is widely considered to be the earliest condensate under the very high C/O ratio during its formation both in EH and EL chondrites and the major carrier of REE as sulfides in solid solution. The following discussion outlines some apparently difficult consequences of a general application of this interpretation. (1) The fundamental signatures of the REE inventories of oldhamite in EH3 and EL3 chondrites is the lack of any similarity to the pattern predicted by Lodders and Fegley (1993) for CaS earliest condensates from a gas of strictly solar abundance at high C/O ratios. (2) Lack of similarities of the REE patterns in oldhamite in EH3 and EL3 albeit oldhamite is considered to be the earliest condensate from a solar gas with chondritic abundances in both EH and EL. (3) Dissimilarity of the REE inventories in oldhamite in EH3 and EL3 might have resulted from different enrichment mechanisms in the two subgroups. EH3 and EL3 reservoirs were at the brink of oldhamite condensation differently REE fractionated with signatures inherited in their CaS earliest condensate or alternatively, condensation of CaS in EH3 and EL3 took place at different total pressures and/or different C/O ratios, respectively. Fifty percent condensation temperatures of CaS and REE sulfides predicted by Lodders and Fegley (1993) and listed in their Table 5 indeed reveal different condensation temperatures calculated for $\log^{-3}$, $\log^{-6}$, and $\log^{-9}$ total pressures. While at $\log^{-3}$ the calculated condensation temperatures for CaS and the REE sulfides LaS, CeS, PrS, NdS, TbS, DyS, HoS, and ErS is 1379 K, at $\log^{-6}$ and $\log^{-9}$ they are different with some REE sulfide species condensing at higher temperature than CaS. (4) Similarity of REE patterns in oldhamite in chondrules and in matrices in the same unequilibrated EH or EL subgroup although CaS in chondrules both in EH3 and EL3 emerged from combined sulfide (mainly CaS-rich) and silicate melts, whereas oldhamite in matrices does not show a similar formational mechanism. Since the individual mainstream REE patterns of oldhamite in both chondrules and matrices in EH3 depict the same positive Eu and Yb anomalies (EH5 Abee exceptionally depicts a negative Eu anomaly like in EL chondrites) whereas oldhamite in EL3 has a negative Eu anomaly both in chondrules and matrices, it is convincing to assume that the REE patterns of oldhamite in the different EH3 or EL3, respectively, did not result from local variation of the total pressure during CaS formation in both chondrite types. Unfortunately, the REE inventories of individual oldhamite grains in the various assemblages with or without graphite overgrowth on sinoite do not disclose further details allowing inspection if the change in C/O ratio at such high reducing conditions is genetically related. Yet, we cannot entirely exclude that semantic changes in the C/O ratio at such high reducing conditions were incapable to induce REE fractionations. The CI-normalized chondritic REE flat patterns of bulk EH3 and EL3 convincingly indicate that the source regions had a similar chondritic REE signature. It is, however, quite logical to conclude that oldhamite in EH and EL chondrites in chondrules and matrices emerged from reservoirs with individual and distinct REE EH- and EL-specific signatures at the brink of their individual nucleation and growth, and definitely was then different from solar, and individually different as well. The process that led to the different REE patterns in oldhamite in EH3 and EL3 chondrites unfortunately further remains unresolved. However, we cannot negate the possibility that the REE abundances in the EH and EL source regions were differently fractionated just at the condensation of oldhamite. REE pattern of oldhamite in EH5 Abee clearly depicts a negative Eu anomaly like in EL3 chondrites although mineralogy and mineral chemistry of this EH chondrites are in full agreement with its classification as an EH chondrite.

Short-Lived Nuclide Chronometry of Enstatite Chondrites

Radiometric investigations of important short-lived systems like $^{129}I/^{129}Xe$ and/or $^{53}Mn/^{53}Cr$ should serve as a critical test for interpretations apt to recognize episodes not discrepant with the petrological and isotopic signatures. $^{129}I/^{129}Xe$ dating of djerfisherite crystals in the EH3 chondrite ALHA 77295 revealed, for example, an age of 1.9–1.1 Ma before the closure of the Shallowater aubrite (King et al. 2013), which can be translated onto an absolute age of 4563.8 ± 0.4 Ma. Authors of this report convincingly interpret this age as evidence for early condensation from the solar nebula

and hence such chondrite could not be placed as a product of a late asteroidal dynamic event. Other enstatite chondrites (Hopp et al. [2016] and references therein) like EH4s Abee, Indarch, and EH5 St. Marks also yield similarly high I-Xe ages comparable to Shallowater of 4562.3 Ma. The result involves an uncertainty encompassing ≈1.5 Ma, a magnitude that calls for a smaller uncertainty to unambiguously negate melting subsequent to condensation. Hence, it is advisable to (1) anchor several short-lived radiometric systems; (2) rely on petrologic phase relations of the coexisting mineral species and their experimentally secured stabilities; (3) check carefully for textural features like eutectic or dendritic troilite-metal intergrowths resulting from expected fast quenching, subsequent to melting; and (4) check for reverse chemical zoning of individual sulfides, niningerite, keilite, and sphalerite in EH3 and alabandite in EL3 characteristic of a thermal episode (Skinner and Luce 1971; Ehlers and El Goresy 1988; El Goresy and Ehlers 1989; and references therein). Yet, the results given above plausibly raise considerable doubt on the melting paradigm.

^{53}Mn-^{53}Cr ages of sphalerites from the primitive EH3 chondrite Sahara 97158 yield 4562.7 ± 0.5 Ma (Trieloff et al. 2013), somewhat higher than Mn-Cr ages of whole rock samples from EH4s Indarch and Abee of 4562.1 ± 1.3 Ma and 4562.5 ± 0.8 Ma, respectively (Lugmair and Galer 1992). On the other hand, the ^{53}Mn-^{53}Cr system of some enstatite chondrites may have been affected by secondary thermally induced disturbances, for example, EH3 Qingzhen, Yamato 691 which have a relatively low Mn-Cr age of 4548 ± 1.9 Ma (all Mn-Cr ages calculated relative to LEW 86010 Pb-Pb age of 4557.8 ± 0.5 Ma and initial ^{53}Mn/^{55}Mn = [1.25 ± 0.07]·10^{-6} and half-life of ^{53}Mn of 3.7 Ma; Lugmair and Galer 1992). Sahara 97158 also shows the same "Qingzhen breakdown reaction of djerfisherite" first reported from both Qingzhen and Yamato-691 (El Goresy et al. 1988). Occurrence of the Qingzhen breakdown reaction of djerfisherite also in three Sahara EH3 chondrites might hint to a common source asteroid also for Qingzhen and Yamato-691. We consider that this metamorphic reaction is crucial in understanding and sifting the episodes an EH3 was subjected to. It may appear difficult to apply it for all EL3 and specifically for MS-17 and MS-177 because djerfisherite was not encountered in them. Impact melting in asteroids is clearly discrepant with the measured undisturbed radiometric ages and with the mineralogy, petrographic fabric, specifically the lack of characteristic textures of dendritic troilite-metal, and cohenite-kamacite intergrowth and reset of short-lived radiometric systems.

Origin of Niningerite in EH3 Chondrites

Recently, Lehner et al. (2013) proposed that niningerite is produced during a sulphidation episode of forsteritic olivine. This reaction calls for considerable changes in the mineral inventory, composition of the FeNi assemblage, increase in fS_2, and the deviation from stoichiometry of troilite. We here recall that the petrology of both EH and EL chondrites is buffered at the Fe/FeS fS_2 curve and evidenced by the close to FeS activity in troilite to unity. Any addition of sulfur would require reaction with the FeNi metal producing monosulfide rims around the metal with FeS activities lower than unity due to cation vacancies in the monosulfide lattice (El Goresy et al. [1988] and references therein). This reaction would also induce formation of perryite rims around the metal. Indeed some metals in EH3 chondrites are coated with thin veneers of perryite (Kallemeyn and Wasson 1986; El Goresy et al. 1988), proposed this reaction to have taken place between nebular H_2S and metal particles. The proposed reaction cannot have taken place after accretion of metal, sulfides, and silicates in parental asteroids otherwise it would have resulted in perryite formation in every metal grain and up to total consumption of the Fe and crystallization of pyrite before any reaction inducing dissociation of forsterite to niningerite + silica (El Goresy and Ehlers 1989). Furthermore, we never encounter forsteritic olivine with a niningerite and silica reaction rims replacing it.

In the following, we now link our discussion to inspect the feasibility of the proposal that unequilibrated EH3 or EL3 chondrites and in particular the metal nodules therein were produced by impact melting in parental proto-asteroids as advocated by, for example, Humayun et al. (2009), Bischoff et al. (2010), and Van Niekerk and Keil (2011) or by pre-accretionary melting in unconstrained source media (Horstmann et al. 2014). Our investigations of 43 nodules outlined in detail in the Metal Nodules section unambiguously demonstrate that none of these nodules ever passed the melt regime. These nodules consist of conglomerates of zoned C-bearing metal pebbles. Such zoning in individual metal pebbles would have been entirely erased if melting had occurred. Both melting proposals solely rely on their own assumptions and interpretation of the concentration of refractory siderophile elements but lack unambiguous petrographic evidence that would convincingly present reliable textural details on the compatibility of the encountered mineral species and their textures with the two proposed and different melting mechanisms along with reliable analytical results, therefore failure to recognize an authentic petrographic nature of the metal, if C-bearing and its

mineral inventory cannot justify applying the refractory siderophile abundances measurement of an inadequately characterized and heterogeneous FeNi metal in the hope to deduce the formational mechanism. We emphasize here that unequilibrated EH3 and EL3 chondrites are primitive in nature and individually consist of textural and mineralogical trichotomous conglomerates of chondrule-rich lithologies, polygonal silicate-rich fragments, and silicate-bearing metal-sulfide nodules (EH3) or metal-rich conglomerates in nodules (EL3) thus convincingly supportive of lithologies with cosmochemical complementarities (see also e.g., Palme et al. 2015; Ebel et al. 2015). The metal nodules in EL3 are fine-scale conglomerates as well, thus setting constraints on their formational mechanisms. Any impact melting would have erased the primordial textural trichotomy of the whole chondrite thus destroying the chondrules in the first place, erase the lithological and chemical complementarities, induce an "igneous-like" texture among silicates, metal-sulfide, and kamacite-cohenite dendritic texture produced during quenching of the impact melts to ambient nebular pressure (latter see Chabot et al. 2010). Melting of any unequilibrated or equilibrated enstatite chondrite at the given low fO_2 and fS_2 with the menagerie of silicate, sulfide, metal, phosphide constituents, and graphite would definitely produce several quenched immiscible liquids. We emphatically remind readers here that melting experiments of Indarch (EH4-5) (McCoy et al. 1999) revealed five coexisting but different immiscible quenched liquids: S-rich, C-rich, Si-rich, P-rich, and a S-rich with significant amounts of nominally lithophile elements, a crucial signature unequivocally not found in any EH3 or EL3 by supporters of the diverse melting episodes or by us. Furthermore, any melting in a metal-, carbon-, sulfide-, phosphide-, and silicate-bearing system would induce distribution of one or more of the light elements C, P, S, and Si between the different immiscible liquids and solid metals (Chabot et al. 2010). This behavior leads further to partitioning of certain minor elements between solid metal and the different immiscible liquids produced. Magnitude of partitioning of the trace elements is not strictly similar for C-, S-, and Si-bearing metal systems. Chabot et al. (2006, 2010) report that the partitioning coefficient for the majority of the refractory siderophile elements increased as the carbon content increased except for the anthracophile elements Cr, Re, and W which are strongly partitioned in the metal liquid. A recent experimental investigation by Chabot et al. (2010) also indicated that only Mo and Rh "show potential week attraction to Si." They also present an additional critical evaluation of the advocated melting scenarios of the reduced enstatite meteorites convincingly suggesting that melts produced from these meteorites could considerably vary in compositions among each other, depending on the temperature and conditions of partial melting. In fact, various melting experiments by Chabot et al. (2006, 2008, 2010) demonstrate that the trace element partitioning behavior can be very sensitive to the composition of the liquid. Hence, inability to recognize petrographic details during microscopic investigations evidencing or negating melting but accompanied by LA-ICPMS studies of the heterogeneous conglomerates in metal nodules and ignoring the possibility that the metal might have emerged as a mixture of accreted heterogeneous solid blebs without melting and possibly contains carbon and sulfur in solid solution can only produce unreliable results. In short, a claimed "pre-accretionary melting episode" should in the first place induce several liquid melts (McCoy et al. 1999), metal-sulfide, kamacte-chenite eutectica and entirely erase the unique primitive metal-sulfide texture we documented in EH3 (Fig. 15) and the conglomerate of zoned pebbles of the metal nodules in EL3 chondrites (Fig. 4).

We strongly emphasize that the suggestion of melting origin for the metal nodules in MS-17, MS-177, and other EL chondrites emerged from the lack of recognition of the conglomerate structure of metal-sulfide nodules in EH3 and metal nodules in EL3. We argue here that our detailed petrographic characterization, the results of McCoy et al. (1999), and meaningful experimental studies by Chabot et al. (2006, 2008, 2010), indeed cast considerable doubts if any melting could have taken place in these primitive EL3 and EH3 chondrites. In contrast, textures and mineral chemistries presented here are indeed not contradicting or negating a solar origin by condensation (Fedkin and Grossman 2006; Grossman et al. 2008).

We maintain that experimental crude practice instead of conducting detailed and skillful petrography can only lead to unrealistic conclusions without any genetic relevance thus deviating to possibly erroneous interpretations. Additional critical issues that lack convincing evidence are:

1. The suggestion that idiomorphic enstatite attached to chondrules is "indicative of crystallization by quenching from impact silicate melts upon fast cooling" (Rubin et al. 1997) is entirely unrealistic, never demonstrated experimentally, and is discrepant with our findings. It is well known among igneous and metamorphic petrologists that enstatite or forsterite quenched from silicate melts in melt experiments or in quenched natural silicate liquids depict dendritic texture as a result of quenching, a texture never reported from any EC allegedly thought to have been produced by

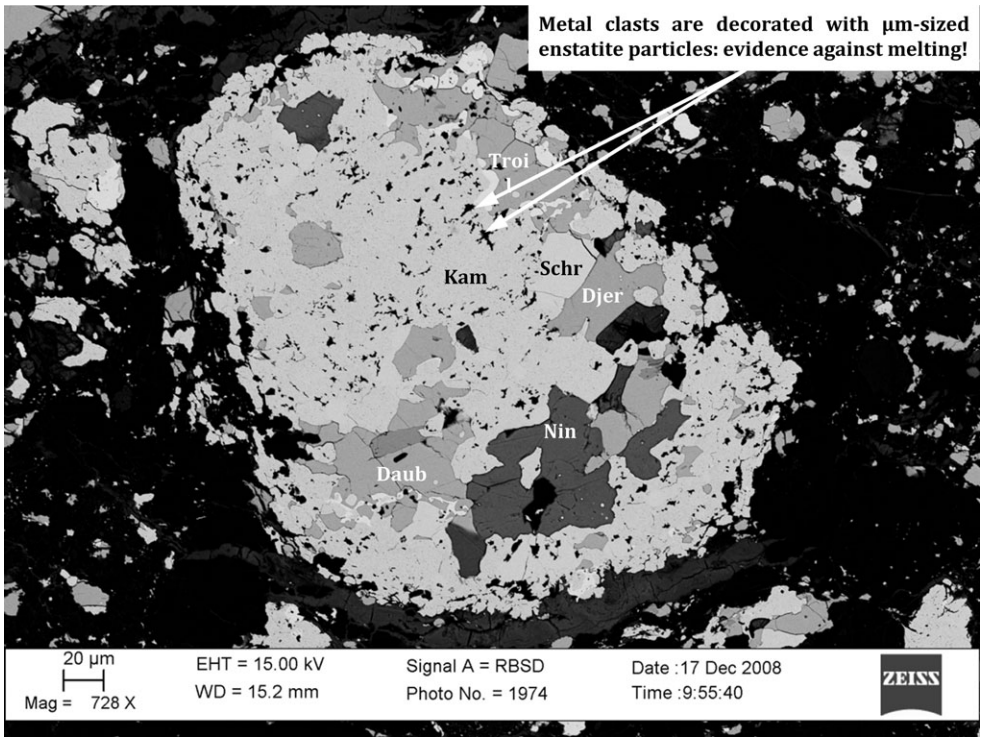

Fig. 15. A BSE-SEM photograph of a typical metal-sulfide nodule in the primitive EH3 chondrite ALHA 77295. The nodule is a multicomponent conglomerate enclosing niningerite (Nin), djerfisherite (Djer), troilite (Troil), abundant kamacite clasts (Kam), daubréelite (Daub), schreibersite (Schr), and perryite. The latter is occurring as bright veneers around some troilite fragments. We emphasize that only kamacite clasts are decorated by a single layer of fine-grained silicate presumably enstatite crystallites. The nodule is quite compact in its interior presumably consolidated by sintering during first stages of accretion. Notice that the outer metal and sulfide clasts are fluffily covering the nodule and not compacted with it. These features were not recognized by advocators of the origin by melting.

quenching of silicate melts; Fig. 4 delivers several lines of convincing evidence against the shock melting or pre-accretionary melting scenarios.

2. How could an impact melting event preserve chondrule morphology and their fluffy delicate sulfide crystallite belts and let instead idiomorphic enstatite nucleate and grow on intact chondrules surfaces?
3. How could sinoite survive the alleged melting episode without amorphization as experimentally demonstrated by Sekine et al. (2006) or its dissociation to N_2 gas and silica thus releasing the N_2 gas in the alleged "pre-accretionary region"?
4. How could sinoite crystallize as abundant stubby or prismatic crystals in solid-state or from alleged immiscible metal liquids with very low N_2 concentration below 0.10% (Hansen and Anderko 1958) in Fe metal produce numerous idiomorphic sinoite crystals up to 22% by volume and then reveal the sinoite-feathery graphite overgrowth texture?
5. How could such a metal liquid or solid produce or conserve upon melting and quenching graphite feathers with considerably variable $\delta^{13}C$ values and heterogeneous N-concentrations?
6. In a way to always serve as nucleation centers for fine-grained graphite platelets of the fanning feathery graphite?
7. How could a metal liquid crystallize graphite platelets with considerably variable $\delta^{13}C$?

Consequently, ignoring these critical parameters and prerequisite details in acquiring the trace element inventory of heterogeneous conglomerates of metal blebs by crude "plowing" a laser beam across inadequately investigated texturally and chemically heterogeneous metal conglomerate (Figs. 4 and 15) by conducting LA-ICPMS in unequilibrated EL3 chondrites and ignoring that the trace element results gained without knowledge of light element compositions (C, S, and P) of the metal constituents can only yield unreliable numbers. Specific depletion in refractory siderophile elements (Re, W, Mo, and Cr) could well have resulted from involvement of one and/or more of the light elements C, Si, S, and P in the metal chemistry inducing their depletion as anthracophile elements in the metal during their formation in the original environment or reservoir.

Description of the textures and constituents of metal nodules presents for the first time clear evidence

that sulfide-metal nodules in the EH3 chondrite ALHA 77295 and metal nodules in the 43 nodules studied here in the EL3 fragments in MS-17 and MS-177 individually consist of either complex structured and heterogeneous conglomerate of kamacite and sulfide clasts (ALHA 77295) or concentrically zoned (Almahata Sitta MS-17 and MS-177) metal pebbles in conglomerates that could not have been produced by metal melting of any kind. Spatial silicate or sinoite decorations of the kamacite clasts (Figs. 4 and 15) in EH3 ALHA 77295 and EL3 could never have survived a melting episode. Concentric zoning of individual pebbles and the decoration of their surfaces and layers by fine-grained sinoite crystallites (Fig. 4) hint to sequential episodes of metal layers growth followed by accretion of one or more solid sinoite dust layers as decoration. Figures 4 and 15 bear witness that the nodule texture has been unaltered since its assembly.

Acknowledgment—We acknowledge the support of Profs. Tomoo Katsura and Hans Keppler, directors of the Bayerische Geoinstitut in Bayreuth, Germany for hosting the senior author and allowance to use of diverse scientific instruments. AE is deeply indebted to the Chinese Academy of Sciences in Beijing, for inviting him to conduct NanoSIMS 50L investigation at the Key Laboratory of Earth and Planetary Physics of CAS, covering his flight, lodging, and living costs. YL was financially supported by Natural Science Foundation of China (41273077, 41521062). We are also indebted to École Polytechnique Féderale de Lausanne, Switzerland for the generous financial support in purchasing Almahata Sitta enstatite chondrite fragments without which this research would not have been completed. We thank Klaus Tschira Stiftung for the support. We are grateful for Prof. Makoto Kimura, Ibaraki University, Mito, Japan for his constructive review that considerably improved the quality of the manuscript. Last but not least, we heartily thank Prof. Timothy Jull, chief Editor of MAPS for his constructive advice and nonbureaucratic handling of our submission.

REFERENCES

Andersen C. A., Keil K., and Mason B. 1964. Silicon oxinitride: A meteoritic mineral. *Science* 146:256–257.

Bischoff A., Horstmann M., Pack A., Laubenstein M., and Haberer S. 2010. Asteroid 2008 TC_3 Almahata Sitta: A spectacular breccia containing many different ureilitic and chondritic lithologies. *Meteoritics & Planetary Sciences* 45:1638–1656.

Buchwald V. F. 1975. *Handbook of iron meteorites*. Berkeley, California: University of California Press. 1148 p.

Campbell A. J., Simon S. B., Humayun M., and Grossman L. 2003. Chemical evolution of metal in refractory inclusions in CV3 chondrites. *Geochimica et Cosmochimica Acta* 67:3119–3134.

Chabot N., Campbell A. J., Jones J. H., Humayun M. and Vern Lauer J. H. 2006. The influence of carbon on trace element partitioning behavior. *Geochimica et Cosmochimica Acta* 70:1322–1235.

Chabot N., Campbell A. J., McDonough W. F., Draper D. S., Agee C. B., Humayun M., Watson H. C., Cottrell E., and Saslow S. A. 2008. The Fe-C system at 5 GPa and implications for Earth's core. *Geochimica et Cosmochimica Acta* 72:4146–4158.

Chabot N., Safko T. M., and McDonough W. F. 2010. Effect of silicon on trace element partitioning in iron-bearing metallic melts. *Meteoritics and Planetary Sciences* 45:1243–1257.

Crozaz G. and Lundberg L. L. 1995. The orogin of oldhamite in unequilibrated enstatite chondrites. *Geochimica et Cosmochimica Acta* 59:3817–3831.

Ebel D., Boyet M., Gannoun A., Hammouda T., Weisberg M. K., and El Goresy A. 2015. Complementary rare-Earth element abundances in enstatite and oldhamite in EH3 chondrites. In *LPSC 2015*, LPI Contribution 1832. Houston, Texas: Lunar and Planetary Institute. 2619 p.

Ehlers K. and El Goresy A. 1988. Normal and reverse zoning in niningerite: A novel key parameter to the thermal histories of EH chondrites. *Geochimica et Cosmochimica Acta* 52:877–862.

El Goresy A. and Ehlers K. 1989. Sphalerite in EH chondrites: Textural relations, compositions, difusion profiles and pressure-temperature histories. *Geochimica et Cosmochimica Acta* 53:1657–1668.

El Goresy A., Yabuki H., Ehlers K., Woolum D., and Pernicka E. 1988. Qinzhen and Yamato-691: A tentative alphabet for the EH chondrites. *Proceedings of the NIPR Symposium on Antarctic Meteorites* 1:65–101.

El Goresy A., Wadhwa M., Nagel H.-J., Zinner E. K., Janicke J., and Crozaz G. 1992. ^{53}Cr-^{53}Mn systematics of Mn-bearing sulfides in four enstatite chondrites. Proceedings, 23rd Lunar and Planetary Science Conference. pp. 331–332.

El Goresy A., Boyet M., and Miyahara M. 2011a. Almahata Sitta EL-3 chondrite fragment: Contrasting oldhamite assemblages in chondrules and matrix and significant oldhamite REE-patterns. *Meteoritics & Planetary Sciences* 46:A36.

El Goresy A., Boyet M., and Miyahara M. 2011b. Almahata Sitta EL-3 chondrite fragment: Contrasting oldhamite assemblages in chondrules and matrx and significant oldhamite REE-patterns. *Meteoritics & Planetary Sciences* 46:A63.

El Goresy A., Lin Y., Miyahara M., Gannoun A., Boyet M., Ohtani E., and Trieloff M. 2015. Evidence for change in C/O ratio during evolution of enstatite chondrites (abstract #1113). In *Goldschmidt Conference*. Prague. 821 p.

Fedkin A. V. and Grossman L. 2006. The fayalite content of chondritic olivine: Obstacle to understanding the condensation of rocky material. In *Meteorites and the early solar system II*, edited by Lauretta D. S., and McSween H. J. Tucson, Arizona: University of Arizona Press. pp. 279–294.

Gannoun A., Boyet M., El Goresy A., and Devoard B. 2011. REE and actinide microdistribution in Sahara 97072 and

ALHA77295 EH3 chondrites. *Geochimica et Cosmochimica Acta* 75:3269–3289.

Grossman L., Beckett J. R., Fedkin A. V., Simon S. B., and Ciesla F. J. 2008. Redox conditions in the solar nebula: Observational, experimental, and theoritical constraints. In *Oxygen in the solar system*, edited by MacPherson G. J., Mittlefehldt D. W., Jones J. H., and Simon S. B. Chantilly, Virginia: Mineralogical Society of America. pp. 93–140.

Hansen M. and Anderko K. 1958. *Constitution of binary alloys*. 2nd ed. New York: McGraw-Hill Book Company. 1305 p.

Hopp J., Trieloff M., and Ott U. 2016. I-Xenon ages of enstatite chondrites. *Geochimica et Cosmochimica Acta* 174: 196–210.

Horstmann M., and Bischoff A. 2014. The Almahata Sitta polymict breccia and the late accretion of asteroid 2008 TC_3. *Chemie der Erde* 140:720–744.

Horstmann M., Humayun M., and Bischoff A. 2014. Clues to the origin of metal in Almahata Sitta EL and EH chondrites and implications for primitive E chondrite thermal histories. *Geochimica et Cosmochimica Acta* 140:720–744.

Humayun M., Keil K., and Bischoff A. 2009. Siderophile elements in metal from North West Africa 2526, an enstatite chondrite partial melt residue (abstract #1744). 40th Lunar and Planetary. Science Conference. CD-ROM.

Kallemeyn G. W. and Wasson J. T. 1986. Compositions of enstatite (EH3, EH4, 5 and EL6) chondrites: Implications regarding their formation. *Geochimica et Cosmochimica Acta* 50:2153–2164.

Keil K. 1968. Mineralogical and chemical relationships among enstatite chondrites. *Journal of Geophysical Research* 73:6954–6976.

Keil K. 2007. Occurence and origin of keilite (Fe 0.5, 0.5 Mg) S in enstatite chondrite impact melt breccias. *Chemie Erde-Geochem*. 76:37–54.

King A. J., Clay P. L., Crowther S. H., Nottigham M., Gilmour J. D., Wieler R., and Busemann H. 2013. Noble gas chronolgy of EH3 chondrite ALHA77295 by closed system stepped etching. LPI Contribution 1719. Houston, Texas: Lunar and Planetary Institute. 2217 p.

Kong P., Mori T., and Ebihara M. 1997. Compositional continuity of enstatite chondrites and implications for hetrogeneous accretion of the enstatite chondrites parent body. *Geochimica et Cosmochimica Acta* 61:4895–4914.

Larimer J. M. and Bartholomay M. 1979. The role of carbon and oxygen in cosmic gases: Some applications to chemistry and mineralogy of enstatite chondrites. *Geochimica et Cosmochimica Acta* 43:1455–1466.

Lehner S. W., Petaev M. I., Zoltow M. Y., and Buseck P. R. 2013. Foration of ningerite by silicate sulfidation in EH3 enstatite chondrites. *Geochimica et Cosmochimica Acta* 101:34–56.

Lin Y. and El Goresy A. 2002. A comparative study of opaque phases in Qingzhen (EH3) and MacAlpine Hills 88136 (EL3): Representatives of EH and EL parent bodies. *Meteoritics & Planetary Sciences* 37:501–511.

Lin Y., El Goresy A., Boyet M., Feng L., Zhang J., and Hao J. 2011. Earliest solid condensates consisting of the assemblage oldhamite, sinoite, graphite and excess ^{36}S in lawrencite from Almahata Sitta MS-17 EL3 chondrite fragment. In *Workshop on Formation of the first solids in the solar system*, Kauai, Hawaii. LPI Contribution No. 1639, p.9040.

Lodders K. and Fegley B. 1993. Lanthanide and actinide chemistry at high C/O ratios in the solar nebula. *Earth and Planetary Science Letters* 117:125–145.

Lugmair G. W. and Galer S. J. G. 1992. Age and isotopic relationships among the angrites Lewis Cliff 86010 and Angra dos Reis. *Geochimica et Cosmochimica Acta* 56:1673–1694.

Lundberg L. L., Crozaz G., Zinner E. K., and El Goresy A. 1989. Rare earth elements and Ca isotopes in the oldhamite in unequilibrated enstatite chondrites (abstract). *Meteoritics* 24:296–297.

McCoy T. J., Dickenson T. L., and Lofgren G. E. 1999. Partial melting of the Indarch (EH4) meteorite: A textural, chemical, and phase relations view of melting and melt migration. *Meteoritics & Planetary Sciences* 34:735–746.

McKinley S. G., Scott E. R. D., and Keil K. 1984. Composition and origin of enstatite in E chondrites. *Journal of Geophysical Research* 89:B567–B572.

Mostefaoui S., Zinner E., Hoppe P., Stadermann F. J., and El Goresy A. 2005. In situ survey of graphite in unequilibrated chondrites: Morphologies, C, N, O, and H isotopic ratios. *Meteoritics & Planetary Science* 40:721–743.

Okamoto H. 1990. C-Fe (carbon-iron). In *binary alloy phase diagrams*, Vol. 1, 2nd ed. edited by Massalski T. B. Materials Park, Ohio: ASM International. pp. 842–848.

Palme H., Hezel D., and Ebel D. 2015. The origin of chondrules: Constraints from matrix composition and matrix-chondrule complementarity. *Earth and Planetary Science Letters* 411:11–19.

Ramdohr P. 1963. The opaque minerals in stony meteorites. *Journal of Geophysical Research* 68:2011–2036.

Ramdohr P. 1973. *The opaque minerals in stony meteorites*. London: Elsevier Publishing Company. 245 p.

Rubin A. E. 1985. Impact melt products of meteoritic material. *Reviews of Geophysics* 23:277–300.

Rubin A. E. and Wasson J. T. 2011. Shock effects in 'EH6' enstatite chondrites and implications for collisional heating of the EH and EL parent asteroids. *Geochimica et Cosmochimica Acta* 75:3757–3780.

Rubin A. E., Scott E. R. D., and Keil K. 1997. Shock metamorphism of enstatite chondrites. *Geochimica et Cosmochimica Acta* 61:847–858.

Sears D. W. G. 1980. Formation of E-chondrites and aubrites—A thermodynamc model. *Icarus* 43:184–202.

Sekine T., He H., Kobayashi T., and Shibata K. 2006. Sinoite (Si2N2O) shocked at pressures of 28 to 64 GPa. *American Mineralogist* 91:463–466.

Skinner B. and Luce F. D. 1971. Solid solution of the type (Ca, Mg, Mn, Fe) S and their use as geothermometers for the enstatite chondrites. *American Mineralogist* 56:1269–1296.

Trieloff M., Storck J. C., Mostefaoui S., El Goresy A., Hopp J., Ludwig T., and Altherr R. 2013. A precise 53Mn-53Cr age of sphalerites from the primitive EH3 chondrite Sahara 97158 (abstract). *Meteoritics & Planetary Science* 48 (Suppl.):5251.pdf.

Van Niekerk D. and Keil K. 2011. Metal/sulfide silicate intergrowth textures in EL3 mreteorites: Origin by impact melting on the EL parent body. *Meteoritics & Planetary Sciences* 46:1484–1497.

Weisberg M. K., and Ebel D. S. 2015. Metal-sulfide nodules in the ALHA 81189 highly primitive EH3 chondrite and the origin of enstatite chondrite components (abstract #2133). 46th Lunar and Planetary Science Conference CD-ROM.

Weisberg M. K. and Kimura M. 2012. The unequilibrated enstatite chondrites. *Chemie der Erde* 72:101–115.